

Habitat heterogeneity and dispersal network structure as drivers of metacommunity dynamics

Davide Bernardi,^{1, 2, 3, *} Alice Doimo,^{1, *} Giorgio Nicoletti,^{4, *} Prajwal Padmanabha,^{5, *}
 Andrea Rinaldo,⁶ Samir Suweis,^{1, 3} Sandro Azalei,^{1, 2, 3} and Amos Maritan^{1, 2, 3, †}

¹*Laboratory of Interdisciplinary Physics, Department of Physics and Astronomy “G. Galilei”, University of Padova, Padova, Italy*

²*National Biodiversity Future Center, Palermo, Italy*

³*INFN, Sezione di Padova, via Marzolo 8, 35131 Padova, Italy*

⁴*International Centre for Theoretical Physics, Trieste, Italy*

⁵*Department of Fundamental Microbiology, University of Lausanne, Switzerland*

⁶*Department of Civil, Environmental and Architectural Engineering, University of Padova, Padova, Italy*

Spatial structure and species interactions jointly shape the dynamics and biodiversity of ecological systems, yet most theoretical models either neglect spatial heterogeneity or sacrifice analytical tractability. Here, we provide a unified microscopic, mechanistic framework for deriving effective metapopulation and metacommunity models from individual-based ecological dynamics on arbitrary dispersal networks. The resulting coarse-grained description features an effective dispersal kernel that encodes both microscopic dynamical parameters and network topology. Based on this framework, we demonstrate exact analytical results for species persistence in both homogeneous and heterogeneous landscapes, including a generalization of the classical concept of metapopulation capacity to non-uniform local extinction rates. Incorporating stochasticity arising from finite carrying capacities, we obtain a reduced one-dimensional description that reveals universal finite-size scaling laws for extinction times and fluctuations. Extending the approach to multiple competing species, we prove that in homogeneous environments monodominance can be avoided only in a fine-tuned, marginally stable coexistence state, and that the classic metapopulation capacity gives only a necessary but not sufficient condition for persistence. We demonstrate that heterogeneous habitats can support stable coexistence, but only above a critical level of heterogeneity. Finally, we outline how additional ecological processes can be systematically incorporated within the same formalism. Together, these results provide analytical benchmarks and a general route for constructing spatially explicit ecological theories based on an interpretable underlying mechanistic foundation.

I. INTRODUCTION

The spatial dimension of ecological dynamics has long been recognized as important [1–13], yet many theoretical studies continue to rely on well-mixed assumptions, where time is the only axis of change [14–19]. Since the early work of Lotka and Volterra, such assumptions have been analytically convenient, but ecologically limiting, as real ecosystems are embedded in heterogeneous landscapes. Incorporating spatial structure into theory is challenging, as it significantly increases complexity. However, a quantitative understanding of the drivers and determinants of species dynamics in spatially extended systems is crucial both to uncover the mechanisms through which biodiversity arises and persists, and to anticipate the impacts of human interventions on ecosystems [20–22].

Multispecies dynamics on landscapes emerge from an interplay between local processes – such as birth, death, competitive or trophic interactions – and global processes – such as colonization and dispersal. Developing models that can disentangle the contributions of these mechanisms, both individually and in combination, is crucial for predicting persistence and coexistence [23–29]. Without such a framework, comparisons to empirical data and the identification of vulnerable species remain elusive.

One route to incorporating space explicitly is through partial differential equation models of population densities in continuous habitats [30, 31]. While powerful, these models are computationally

* Equal contribution

† Correspondence: amos.maritan@unipd.it

demanding and analytically challenging, especially when space is not homogeneous. A more tractable intermediate framework is provided by metapopulation and metacommunity theory, in which the landscape is represented as a set of discrete habitat patches connected by dispersal [24, 32]. Within patches, populations are assumed to be well-mixed, enabling models that capture both local interactions and between-patch connectivity. This abstraction has proved fruitful: in the single-species case, metapopulation models yield clear metrics for persistence, such as the metapopulation capacity introduced by Hanski and Ovaskainen, which links survival thresholds to landscape connectivity [4, 33]. However, extending these approaches to multiple interacting species is more challenging. While several classical paradigms of metacommunity theory – species sorting, patch dynamics, mass effects, and neutrality – provide conceptual structure, empirical systems often exhibit mixtures of these processes, and generalizable measures for multispecies persistence remain limited.

Statistical physics provides a complementary perspective, aiming to describe complex systems through coarse-grained variables and emergent laws rather than microscopic detail. May's seminal analysis of random community matrices [34] demonstrated that tools from random matrix theory could set a null expectation for stability in large ecosystems [14, 17, 35, 36]. Since then, methods drawn from spin-glass theory, disordered systems, and mean-field dynamics have been used to study ecological communities [16, 37–41]. These approaches naturally emphasize universality: details of individual species and interactions can be abstracted away, allowing analysis in terms of scaling laws, phase transitions, and macroscopic stability criteria. These approaches identify broad patterns, such as phase transitions between stable and unstable community states, but they too have often relied on well-mixed assumptions that neglect spatial heterogeneity.

Metacommunity theory provides a natural meeting point between these perspectives. Single-species metapopulation models already display phase transitions between extinction and persistence, with control parameters determined by landscape connectivity [4, 42]. In systems with multiple interacting species, dispersal shapes collective dynamics and may promote nonequilibrium behaviors [25, 27, 43–46]. Heterogeneity in habitat quality, dispersal pathways, and competition among species resembles the quenched disorder studied in statistical physics. These parallels suggest that techniques from disordered systems, finite-size scaling, and non-equilibrium statistical mechanics are well-suited for advancing ecological theory.

Here, we unify, generalize, and provide a more rigorous theoretical grounding for recent approaches for deriving effective metacommunity theories from the bottom up, that integrate species-specific traits and processes while explicitly accounting for landscape structure [42, 47, 48]. This approach offers a balance between interpretability and tractability: the resulting models provide reduced descriptions that retain a clear link to the underlying ecological mechanisms. Such a connection is crucial when testing model predictions against empirical data – such as species distributions across space – and when tracing these patterns back to landscape features and species traits, ideally disentangling their respective contributions.

The article is organized as follows. In Section II, we present the core ideas in a simplified scenario involving a single species and basic ecological processes: space-limited local demography and network-based dispersal and colonization [42]. We then show analytical results for single-species persistence in arbitrarily structured landscapes, extending the classical concept of metapopulation capacity to heterogeneous habitats where local extinction rates may vary (Section III). Next, in Section IV, we study the effect of stochasticity [48]. We then introduce interspecific interactions into the model in Section V, beginning with competition [47]. In Section VI, we derive further analytical results on the coexistence of species in both homogeneous and heterogeneous habitats. Finally, we show in Section VII how additional ecological processes can be systematically included, paving the way for metacommunity models that strike a balance between reduced complexity and a mechanistic link to the underlying ecological processes. Proofs of theorems in the main text are presented in the appendices.

II. METAPOPULATION MODELS FROM MICROSCOPIC DYNAMICS

We introduce a microscopic description of a metapopulation model on arbitrary networks [42]. We first consider the dynamics of a single species in a dispersal network of N habitat patches, each with a finite

number M_i of colonizable sites. The network is described by a weighted adjacency matrix \hat{A} , whose elements A_{ij} denote the strength of the dispersal from the i -th habitat to the j -th one, with $A_{ii} = 0$. In this setting, we describe all ecological processes through individual-based transitions [49, 50]. We assume that each patch is inhabited by a settled population that does not move. If we denote a settled individual in patch i by S_i , we assume that each individual can die with a patch-dependent death rate $e_i > 0$.

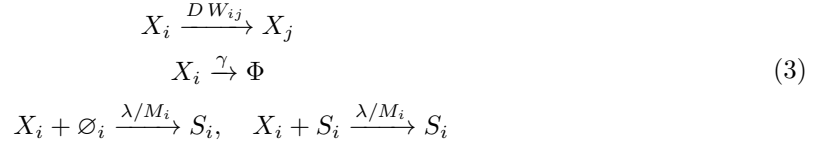


where \emptyset denotes an empty site in the same patch.

Although settled individuals do not move, they can produce new individuals of the same species that explore the network and attempt to colonize other patches. We denote one such explorer in the i -th patch with X_i . In some ecological contexts, this distinction between settled populations and explorers has a direct biological interpretation – for example, plants and their seeds, or sessile adults and dispersing larvae. In other contexts, it serves as a conceptual distinction reflecting differences in the life histories or time scales of ecological processes, which are fundamental for deriving general metapopulation models from microscopic dynamics, as we will see. Explorers' birth is governed by the reaction



where c_i acts as a birth rate for the explorers from patch i , and C_{ij} denotes the feasibility of exploration from patch i to patch j . Similarly, explorers can move between two patches with a rate $D_{ij} = DW_{ij}$, where D is a baseline exploration rate and $W_{ij} \neq 0$ if and only if explorers can move directly from the i -th habitat to the j -th habitat patch. We will always make the assumption that $W_{ij} = A_{ij}$, i.e., that explorers can only move one step at a time along the dispersal network edges. However, our results can be applied to other scenarios, such as one where multiple steps are taken at once. Then, explorers die with a rate γ or attempt to colonize the patch they are in with a rate λ . We write these reactions as



where Φ denotes an empty unbounded space for explorers. The rate λ/M_i appearing in Eq. (3) takes into account both the rate at which explorers attempt colonization, λ , and the fact that, when they do, they can choose one of the M_i sites of patch i .

We denote the number of individuals with $[\cdot]$ so that the state of the model is fully specified by $([\vec{S}], [\vec{X}]) = ([S_1], \dots, [S_N], [X_1], \dots, [X_N])$ since, at all times, we have that $[S_i] + [\emptyset] = M_i$ for all i . In particular, we are interested in the density of individuals in each patch i , $p_i = [S_i]/M_i \in [0, 1]$, and we first consider the limit in which the number of colonizable sites M_i is large, so we can ignore stochastic effects. We will relax this assumption later. We obtain the equations

$$\begin{aligned} \dot{p}_i &= -e_i p_i + \lambda(1 - p_i)x_i \\ \dot{x}_i &= -(\lambda + \gamma)x_i + \sum_{j=1}^N p_j c_j \frac{M_j}{M_i} C_{ji} + \frac{D}{M_i} \sum_{j=1}^N (x_j M_j W_{ji} - x_i M_i W_{ij}) \end{aligned} \quad (4)$$

where we also introduced for convenience the rescaled number of explorers $x_i = [X_i]/M_i$. Equation (4) also corresponds to the evolution of the averages

$$\begin{aligned} \langle S_i \rangle_p(t) &= \sum_{[S_i]=0}^{M_i} [S_i] p([S_i], t) \\ \langle X_i \rangle_p(t) &= \sum_{[X_i]=0}^{\infty} [X_i] p([X_i], t) \end{aligned}$$

and can be seen as the first order of the Kramers-Moyal expansion of the master equation for the probability $p([\vec{S}], [\vec{X}], t)$, where $[\vec{S}] = ([S]_1, \dots, [S]_N)$ with the set of reactions in Eqs. (1) to (3).

A. Fast-exploration regime

Although Eq. (4) fully describes the deterministic limit of our microscopic model, we now assume that only settled individuals are visible and seek to derive an effective metapopulation dynamics involving only the settled population density. Specifically, we take the limit in which explorers are much faster than the local dynamics on patches [42] (see Figure 1a). We perform a quasi-stationary approximation by setting $\dot{x}_i = 0$, which enables us to write the relation

$$\lambda x_i = \sum_{j=1}^N \sum_{k=1}^N p_j c_j \frac{M_j}{M_i} C_{jk} F_{ik}^{-1} \quad (5)$$

where F_{ij}^{-1} is a shorthand notation for the elements of the inverse of the matrix

$$F_{ij} = \left(1 + \frac{\gamma}{\lambda}\right) \delta_{ij} + \frac{D}{\lambda} \left(\delta_{ij} \sum_{k=1}^N W_{ik} - \frac{M_j}{M_i} W_{ji} \right). \quad (6)$$

Eq. (6) only depends on two dimensionless parameters,

$$f = \frac{D}{\lambda}, \quad g = \frac{\gamma}{\lambda}, \quad (7)$$

with f quantifying the exploration efficiency in terms of how many patches are visited before a colonization attempt and g the explorers' lifespan. Clearly, if $f \ll 1$, i.e. $D \ll \lambda$, explorers will remain close to the originating patch. On the other hand, if $D \gg \lambda$ they will explore far-away patches before settling on one. Similarly, $g \ll 1$ denotes the limit in which explorers will survive long enough to always attempt colonization before dying, whereas $g \gg 1$ makes exploration harder.

By inserting Eq. (5) into the rate equation for the settled population, Eq. (4), we end up with the effective evolution

$$\dot{p}_i = -e_i p_i + (1 - p_i) \sum_{j=1}^N c_j K_{ij} p_j \quad (8)$$

where we introduced the kernel matrix

$$K_{ij} = \frac{M_j}{M_i} \sum_{k=1}^N C_{jk} F_{ik}^{-1} \quad (9)$$

which describes the effective colonization rate from patch j to patch i due to the effect of the explorers. As expected, large patches influence smaller ones more through the pre-factor M_j/M_i . Importantly, the effective dynamics, through the kernel \hat{K} in Eq. (9), summarizes the dependence of the detailed reactions and the network topology, showing how the microscopic features of the model are instrumental in determining the properties of the metapopulation.

B. Kernel-based encoding of structure and dynamics

In order to understand the properties of the kernel, we need explicitly to invert the matrix \hat{F} in Eq. (6). To do so, we assume that the matrix

$$L_{ij} = \delta_{ij} \sum_{k=1}^N W_{ik} - W_{ji} \quad (10)$$

is diagonalizable, i.e. $\hat{L} = \hat{V}\hat{\Omega}\hat{V}^{-1}$, where $\hat{\Omega}$ is a diagonal matrix. We note that if $W_{ij} = A_{ij}$ (the adjacency matrix introduced above), then Eq. (10) corresponds exactly to the standard combinatorial Laplacian, with $\sum_k A_{ik} := q_i$ as the out-degree of patch i . Other relevant choices are possible, such as $W_{ik} = A_{ik}/q_i$, which corresponds to the random walk Laplacian.

In general, we will focus on the scenario where explorers move according to the dispersal network described by \hat{A} . Then, we can immediately invert \hat{F} , which is diagonal in the eigenspace of \hat{L} , to find the explicit form of the kernel:

$$K_{ij} = \frac{M_j}{M_i} \sum_{k=1}^N C_{jk} \sum_{l=1}^N \frac{V_{kl}(V^{-1})_{li}}{1+g+f\omega_l} \quad (11)$$

where ω_k is the k -th eigenvalue of \hat{L} . In suitable cases, Eq. (11) can be interpreted as a weighted sum over all possible paths between two patches [42]. Furthermore, it manifestly incorporates both dynamical features - through f and g - and topological ones - through \hat{C} and the eigenspace of \hat{L} .

Several choices for the feasibility of exploration C_{ij} are possible as well, which should depend, in general, on the efficiency of exploration f . In particular, if $f \rightarrow \infty$, we assume that there exists a maximal explorability ξ , which corresponds to the maximal dispersal capacity of the species. Conversely, if $f \rightarrow 0$, exploration should not be possible, and C_{ij} should vanish. Hence, we expect that

$$C_{ij}(f) \xrightarrow{f \ll 1} 0, \quad C_{ij}(f) \xrightarrow{f \gg 1} \xi. \quad (12)$$

The simplest choice would be to set $C_{ij} \propto \delta_{ij}$, so that explorers are created in the same patch. In order to avoid self-colonization - which is particularly relevant if $f \ll 1$ - another option is to take $C_{ij} \propto A_{ij}$, so that explorers are created in neighboring patches. This choice is equivalent to assuming that explorers need to take at least one exploration step before attempting colonization. Then, a simple parametric form is

$$C_{ij} = \frac{\xi}{1+1/f} A_{ij}, \quad (13)$$

but our approach naturally allows for other choices as well, leading to a vast array of possible phenomenologies.

In Figure 1b, we show how the kernel changes with the structure of the dispersal network. We consider three exemplary topologies. In a ring network, the kernel decays exponentially with the network distance d_{ij} between patch i and patch j . The characteristic decay length increases with f , suggesting a direct relation between exploration efficiency and the average dispersal distance of the species. However, in more complex topologies, the kernel elements are not solely a function of the network distance. This effect becomes especially relevant at large f , and it is a direct consequence of the fact that the kernel encodes contributions from all possible paths between habitat patches. In particular, in Figure 1b, we also consider a small-world dispersal network, introducing long-range connections between patches that may be otherwise very far apart, and a Barabasi-Albert topology, where a few patches behave as hubs and connect to a large number of other nodes.

C. Metapopulation persistence

In full generality, Eq. (8) admits a trivial solution where the focal species is extinct, i.e. $p_i = 0$ for all patches. We can characterize the linear stability of this solution by computing the leading eigenvalue of the Jacobian matrix

$$J_{ij}(\vec{p} = 0) = \left. \frac{\partial \dot{p}_i}{\partial p_j} \right|_{\vec{p}=0} = -e_i \delta_{ij} + c_j K_{ij}.$$

In particular, we can first focus on the case considered by previous works in which all patches are equivalent, so that $M_i = M$, $e_i = e$, and $c_i = c$. Then, we find that the extinct state is unstable if and

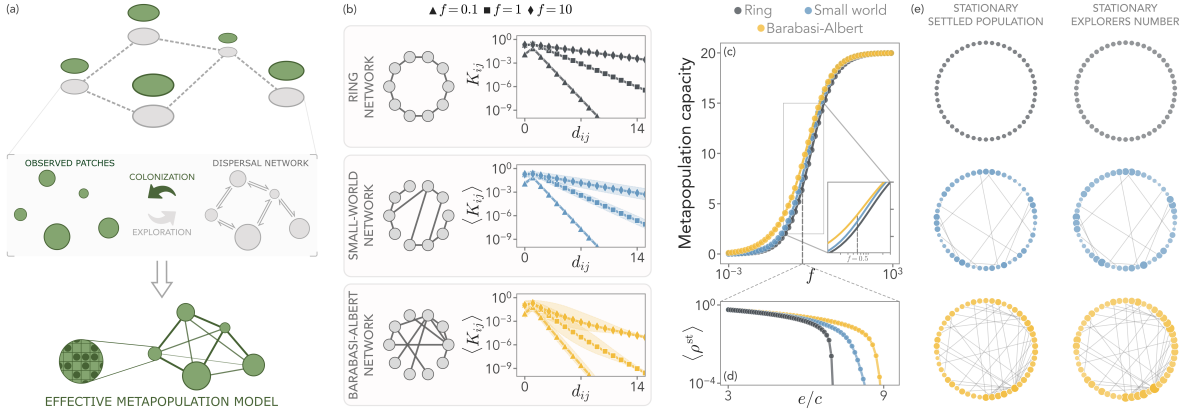


FIG. 1. (a) Sketch of the model. We consider the dynamics of a settled population, which resides in habitat patches, and of explorers that move along a dispersal network and attempt colonization. In the fast-exploration regime, this leads to an effective metapopulation model with an explicit colonization kernel. (b) The colonization kernel depends manifestly on the topology of the dispersal network. In general, it is not a function of the network distance d_{ij} alone, but rather depends on all paths connecting two habitat patches. (c-e) The metapopulation capacity, which determines a species' survival ability, depends on both the exploration efficiency f and the network topology. In particular, more heterogeneous dispersal networks are more advantageous at intermediate and low f , affecting the stationary population and explorers (panels (d) and (e)). Figure adapted from [42].

only if

$$\lambda_M > \frac{e}{c} \quad (14)$$

where λ_M is the maximum eigenvalue of the kernel \hat{K} , and it is referred to as the metapopulation capacity of the landscape [4].

In Figure 1c, we show that the structure of the dispersal network directly affects the metapopulation capacity. The survival of a species tends to increase with the heterogeneity of the network, especially at intermediate and low f , where the topological features may help a species colonize and survive.

III. EXACT RESULTS ON THE METAPOPULATION CAPACITY OF A FOCAL SPECIES

We now prove several exact results on the focal species persistence based on Eq. (8). The proofs of all theorems and corollaries are in Section A. In the following, we can set $c_i = 1$ for all i , which is equivalent to a rescaling of the colonization kernel, and does not restrict the generality of the results.

A. Generalized metapopulation capacity in heterogeneous habitats with non-uniform local extinction rates

We first generalize the classic result on the metapopulation capacity of a landscape from Section II C, which holds only for the case of a patch-independent extinction rate. To this end, we leverage the fact that the entries of the colonization kernel are all positive if the graph has a single connected component. However, we can adopt the even more general assumption that \hat{K} is irreducible. Given the assumption stated above,

Theorem 1. *Given the following metapopulation dynamics*

$$\dot{p}_i(t) = -e_i p_i(t) + (1 - p_i(t)) \sum_{j=1}^N K_{ij} c_j p_j(t), \quad (15)$$

where $e_i > 0$ and the kernel matrix \hat{K} is irreducible. Let $\hat{\mathcal{E}}$ be the matrix with elements $\mathcal{E}_{ij} = e_i \delta_{ij}$, and $\hat{\mathcal{C}}$ be the matrix with elements $\mathcal{C}_{ij} = c_i \delta_{ij}$. Then, the generalized landscape matrix

$$\hat{\mathcal{M}} = \hat{K} \hat{\mathcal{C}} \hat{\mathcal{E}}^{-1} \quad (16)$$

is also irreducible, and has a Perron-Frobenius positive eigenvalue $\lambda_{\max} > 0$. Then, for all non-trivial initial conditions, $\vec{p}(0) \neq 0$, and $p_i(0) \in [0, 1]$, $\lim_{t \rightarrow \infty} \vec{p}(t) = 0$, i.e., $\vec{p} = 0$ is globally stable if $\lambda_{\max} < 1$ and unstable if $\lambda_{\max} > 1$.

This theorem leads to the following statement:

Corollary 1. *When $\lambda_{\max} > 1$, the stationary state of Eq. (15) is non-trivial. Specifically, if a non-trivial stable stationary state exists, then the population is strictly positive in all patches, i.e. $p_i > 0, \forall i$.*

We now observe that the classical result on the metapopulation capacity of Hanski and Ovaskainen, assuming an exponentially decaying dispersal kernel [4], can be derived as a corollary of Theorem 1:

Corollary 2. *Let*

$$e_i = \frac{e}{A_i}, \quad c_i = c A_i, \quad \text{and} \quad K_{ij} = e^{-\alpha d_{ij}}, \quad (17)$$

where A_i denotes the area of patch i and d_{ij} the distance between patches i and j . Then, the long-term behavior of Eq. (15) is non-trivial if $\delta = e/c < \lambda_M$, where λ_M is the largest eigenvalue of the symmetric landscape matrix $\mathcal{M}_{ij}^H \equiv A_i e^{-\alpha d_{ij}} A_j$.

While the rigorous proof of both corollaries is provided in Section A, we immediately have that Eq. (14) can be rewritten as $\lambda_M c e^{-1} > 1$, in agreement with Theorem 1. A noteworthy implication of Theorem 1 is that the local extinction and colonization rates of every landscape patch contribute to the leading eigenvalue and thus affect the species persistence threshold. Consequently, this threshold is a global property of the system rather than being determined by a few particularly favorable patches. Thus, we define the generalized metapopulation capacity, λ_{\max} , as the maximum eigenvalue of the matrix $\hat{K} \hat{\mathcal{C}} \hat{\mathcal{E}}^{-1}$.

B. Stability and uniqueness of steady-state solutions in homogeneous habitats

We now consider the special case of systems that are spatially homogeneous, a scenario in which further exact results can be proven. Note that in such a setting, $e_i = e \forall i$. Then, the stability of both trivial (global extinction) and non-trivial steady states can be studied explicitly. Furthermore, we prove that the non-trivial steady state is unique. Strict spatial homogeneity implies dynamics taking place in a finite d -dimensional lattice $\Lambda = \{1, 2, \dots, N-1\}^d$ with spacing set equal to 1, periodic boundary conditions, and K_{ij} can depend only on $j - i \bmod N, \forall i, j \in \Lambda$. However, we are able to prove the following theorem under the less restrictive hypothesis that \hat{K} is irreducible and that row sums are independent of the row index.

Theorem 2. *Consider the metapopulation dynamics:*

$$\dot{p}_i = -e p_i + (1 - p_i) \sum_j K_{ij} p_j. \quad (18)$$

Assume that \hat{K} is irreducible and that its row sums are constant $\tilde{K}_0 = \sum_j K_{ij}$. Then,

- When $e > \tilde{K}_0$, the global extinction state is globally stable; a non-trivial steady state is not feasible.
- When $e < \tilde{K}_0$, the global extinction state is unstable; the non-trivial, spatially-uniform stationary solution is unique and locally stable.

In Section A we provide both a proof for the general case of a constant-row matrix, as in the theorem's statement, and an alternate proof valid only in the translation-invariant case, which uses explicit Fourier modes. Previous works showed a stronger result, the global stability of the non-trivial state [51, 52]. The proofs of Theorem 2 reported in Section A are based on simpler, self-contained arguments.

IV. STOCHASTIC METAPOPULATION DYNAMICS AND FINITE-SIZE EFFECTS

Having established the basic framework and illustrated it with both numerical and exact results, we now examine the effects of a finite patch size M_i , which acts as a finite carrying capacity and introduces fluctuations in the settled population. Rather than simply adding demographic noise to Eq. (8), a consistent incorporation of stochastic effects within our framework requires returning to the underlying microscopic model and moving beyond the first order Kramers-Moyal expansion we performed before.

A. From deterministic dynamics to stochastic fluctuations

We begin with the microscopic model introduced in Section II, but we make some simplifications for analytical tractability. We assume there is no inherent explorer death ($\gamma = 0$), that all patches have the same carrying capacity ($M_i = M$), that explorer creation reflects the network ($C_{ij} \propto A_{ij}$), and without loss of generality, $c = 1$. We set $p_i = [S_i]/M \in [0, 1]$ and $x_i = [X_i]/M$. To analyze the stochastic dynamics, we consider the corresponding master equation and perform a Kramers-Moyal expansion, using the inverse carrying capacity $1/M$ as the expansion parameter. Truncating the expansion at first order recovers the deterministic model discussed above, while extending it to second order yields the following Fokker-Planck equation [48]:

$$\partial_t \mathcal{P}(\vec{z}, t) = - \sum_i \partial_i [\mathcal{A}_i(\vec{z}) \mathcal{P}(\vec{z}, t)] + \frac{1}{2M} \sum_{i,j} \partial_i \partial_j [\mathcal{D}_{ij}(\vec{z}) \mathcal{P}(\vec{z}, t)], \quad (19)$$

where $\vec{z} = (\vec{p}, \vec{x})$ is the $2N$ -dimensional state vector, $\vec{A}(\vec{z})$ is the drift vector

$$\begin{aligned} \mathcal{A}_i &\equiv \mathcal{A}_i^p = \lambda x_i (1 - p_i) - e_i p_i, \quad i \leq n \\ \mathcal{A}_i &\equiv \mathcal{A}_i^x = D \sum_j (W_{ji} x_j - W_{ij} x_i + C_{ji} p_j) - \lambda x_i, \quad i > n, \end{aligned} \quad (20)$$

where we assume that $W_{ij} = A_{ij}$ and $\hat{\mathcal{D}}$ is a $2N \times 2N$ diffusion matrix with the block structure

$$\hat{\mathcal{D}}(\vec{z}) = \begin{pmatrix} \hat{\mathcal{D}}^{pp} & \hat{\mathcal{D}}^{px} \\ \hat{\mathcal{D}}^{xp} & \hat{\mathcal{D}}^{xx} \end{pmatrix}, \quad (21)$$

where the $N \times N$ blocks are

$$\begin{aligned} \mathcal{D}_{ij}^{pp} &= [e_i p_i + \lambda x_i (1 - p_i)] \delta_{ij} \\ \mathcal{D}_{ij}^{px} &= \mathcal{D}_{ij}^{xp} = -\lambda x_i (1 - p_i) \delta_{ij} \\ \mathcal{D}_{ij}^{xx} &= \left[\sum_k (p_k C_{ki} + x_i W_{ik} + x_k W_{ki}) + \lambda x_i \right] \delta_{ij} - (x_i W_{ij} + x_j W_{ji})(1 - \delta_{ij}). \end{aligned} \quad (22)$$

As expected, the diffusion term of (19) vanishes in the limit of large local capacity $M \rightarrow \infty$. Although the Fokker–Planck equation represents a significant dimensional simplification compared to the full master equation, its form still poses several challenges, as the drift and diffusion terms, Eqs. (20) and (21), are complex and coupled both within and across patches. To simplify, we consider a fully connected dispersal network, i.e. , an adjacency matrix $A_{ij} \propto 1/N(1 - \delta_{ij})$, representing homogeneous habitat patches. Then, we perform a time-scale separation and write a one-dimensional stochastic differential equation for the effective density of settled individuals p :

$$\dot{p} = \tilde{\mathcal{A}}(p) + \sqrt{\frac{1}{M} \tilde{\mathcal{D}}(p)} \xi(t) \quad (23)$$

where $\xi(t)$ denotes a Gaussian white noise, while $\mathcal{A}(p)$ and $\tilde{\mathcal{D}}(p)$ are the effective drift and diffusion coefficients, respectively (see Section C for details on their derivation and explicit forms). Equation (23) is defined on the domain $0 < p \leq 1$, with $p = 0$ as an absorbing boundary corresponding to global extinction and $p = 1$ as a reflecting boundary representing the maximum local capacity. In the deterministic limit, Eq. (23) recovers the metapopulation capacity λ_M , which separates extinction from persistence, in agreement with Section II C and Theorem 1. For finite M , extinction is inevitable as $t \rightarrow \infty$, and $p_{\text{st}} = 0$ is the only true stationary state. Nonetheless, the condition $e < \lambda_M$ still defines a survival regime corresponding to a long-lived metastable state, where extinction occurs only through large fluctuations. Simulations of the full microscopic model show excellent agreement with the one-dimensional reduction Eq. (23) in the survival regime, and only minor deviations in the mean-driven extinction regime that do not affect the qualitative behavior (Figure 2a-b).

B. Finite-size scaling of the extinction-time distribution

Since the noise amplitude scales as $1/M$, systems with smaller carrying capacities experience stronger intrinsic fluctuations and a higher probability of noise-induced extinction. We study the survival probability $S(t|M)$ at a finite system size M , focusing on the deterministic transition point ($e/c = \lambda_M$), where we expect a possible critical behavior. Indeed, numerical simulations of Eq. (23) reveal that the survival probability collapses as:

$$S(t|M) \sim f(t M^\phi), \quad (24)$$

shown in Figure 2c-d. This behavior indicates that the critical regime exhibits classical finite-size scaling with a universal exponent $\phi = -1/2$. The scaling behavior of the survival probability and of the first two moments of the extinction time distribution can be investigated analytically by studying the scaling behavior of the backward Fokker-Planck operator (see Section C). This analysis yields

$$S = t^{-\alpha} \hat{S}(t M^\phi, p_0 M^\gamma, \Delta M^\eta), \quad \langle T \rangle = M^\beta \hat{T}_1(p_0 M^\gamma, \Delta M^\eta), \quad \langle T^2 \rangle = M^\delta \hat{T}_2(p_0 M^\gamma, \Delta M^\eta) \quad (25)$$

where $\Delta = (\lambda_M - e/c)/\lambda_M$ quantifies the distance from the deterministic transition threshold, and p_0 is the initial condition. The exponents are connected through the scaling relations $\beta = -\phi(1 - \alpha)$, $\delta = -\phi(2 - \alpha)$. Their numerical values are reported in Table I (Section C). Importantly, these exponents characterize a specific universality class of noise-driven extinction dynamics. Modifications to the underlying individual reactions may change the functional form of the SDE and alter the critical exponents. Therefore, analyzing such scaling behaviors can provide a means to identify different underlying ecological mechanisms, using the present framework as a template.

C. Linear approximation in the metastable regime

Building on the effective one-dimensional dynamics derived in the previous section, we show that key features of stochastic extinction can be described using simplified observables that retain ecological

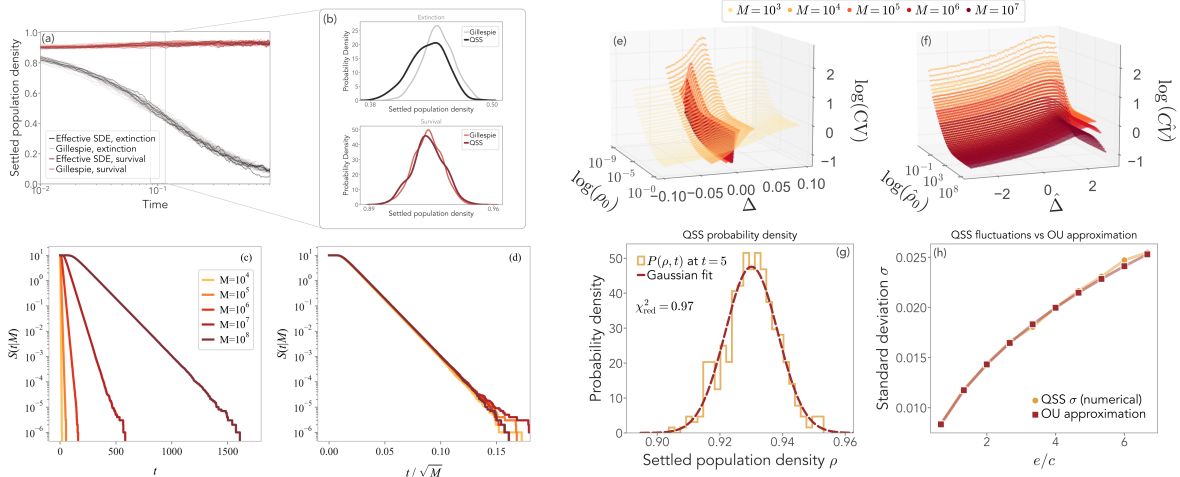


FIG. 2. (a–b) Comparison of stochastic trajectories from the effective quasi-stationary SDE Eq. (23) and the full Gillespie simulation in the survival and extinction regimes. (c–d) Finite-size scaling of the survival probability at criticality: (c) raw curves of survival probability as functions of time for different carrying capacities M , (d) collapse under the scaling ansatz Eq. (24). The initial condition is fixed at $p_0 = 1/2$. Averages are obtained over 10^7 numerical realizations of the dynamics in Eq. (23). (e–f) Coefficient of variation of extinction times as a function of initial condition p_0 and deviation from criticality Δ for different values of the local carrying capacity M : (e) unscaled, (f) rescaled using finite-size scaling of the first two moments Eq. (25). Averages are obtained over 10^7 numerical realizations of the dynamics in Eq. (23). (g–h) Fluctuations in the metastable regime: (g) distribution of settled densities obtained from 350 independent realizations with Gaussian fit; (h) standard deviation σ vs. e/c , compared with the analytical estimate based on the Ornstein–Uhlenbeck (OU) approximation. The numerical values of σ are obtained from Gaussian fits to distributions built from 250 independent realizations. Adapted from ref. [48].

interpretability. In particular, we analyze the coefficient of variation (CV) of extinction times, defined as the ratio between the standard deviation and the mean, $CV(T) = \sqrt{\langle T^2 \rangle - \langle T \rangle^2} / \langle T \rangle$. This dimensionless measure of relative variability exhibits a finite-size scaling collapse, as expected, and develops a pronounced maximum at a finite rescaled distance from criticality $\tilde{\Delta} = \Delta\sqrt{M} > 0$. This peak, located within the metastable survival regime, signals a fluctuation-driven transition associated with maximal uncertainty in extinction time (Figure 2e–f). In this regime, extinctions are caused by a large fluctuation from the metastable state, which can be captured by a linear approximation of the effective dynamics Eq. (23) around the deterministic fixed point. This effective Ornstein–Uhlenbeck process (Section C) approximation closely agrees with numerical simulations (Figure 2g–h), demonstrating how a coarse representation of the stochastic system can be used effectively to link measurable population-level statistics to underlying ecological mechanisms.

V. INTERSPECIES INTERACTIONS IN COMPETITIVE METACOMMUNITIES

We now shift our focus from single-species metapopulation models in different settings to multi-species metacommunity models by incorporating interspecies interactions. As a starting point, we focus on the paradigmatic case of purely competitive species, since competition for space and resources is a pervasive and fundamental driver of ecological exclusion [2, 53–56].

We consider the same ecological reactions as in Section II, and add a species index, using the convention that species are indicated by Greek indices and patches by Latin indices. Hence, a settled individual belonging to species α located within patch i will be indicated with $S_{\alpha i}$. The reaction

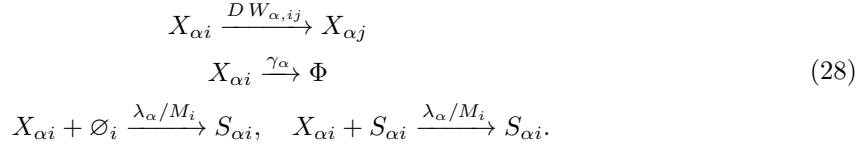
involving settlers introduced in Section II naturally generalizes to



where $e_{\alpha i}$ denotes the local death rate of species α in patch i . Reactions describing the generation of explorers are straightforward generalizations of the single-species case:



The explorers' reactions are also analogous to the single-species case:



An important difference with respect to the single-species case is that explorers of different species compete for the same empty spaces, which will lead to an interaction term in the effective metacommunity equations.

For simplicity, we assume that $\gamma_\alpha = 0$, $C_{\alpha,ij} = h_\alpha A_{\alpha,ij}$, and $W_{\alpha,ij} = A_{\alpha,ij}$. Under these assumptions, the set of microscopic reactions above leads to the following rate equations for the settler and explorer densities, which we indicate with $p_{\alpha i} = [P_{\alpha i}]/M_i$ and $x_{\alpha i} = [X_{\alpha i}]/M_i$, respectively:

$$\dot{p}_{\alpha i} = -e_{\alpha i} p_{\alpha i} + \lambda_\alpha \left(1 - \sum_{\beta=1}^S p_{\beta i} \right) x_{\alpha i} \quad (29)$$

$$\dot{x}_{\alpha i} = - \left(\lambda_\alpha x_{\alpha i} - h_\alpha \sum_{j=1}^N A_{\alpha,ji} c_{\alpha j} p_{\alpha j} \frac{M_j}{M_i} \right) + D_\alpha \sum_{j=1}^N \left(A_{\alpha,ji} x_{\alpha j} \frac{M_j}{M_i} - A_{\alpha,ij} x_{\alpha i} \right). \quad (30)$$

As in Section II, we assume that exploration occurs on time scales much shorter than those of the settled population; therefore, we set $\dot{x}_{\alpha i} = 0$. This quasi-stationary assumption leads to

$$\lambda_\alpha x_{\alpha i} = h_\alpha \sum_{j,k=1}^N \sum_{\beta=1}^S (\hat{F}^{-1})_{ik}^{\alpha\beta} A_{\beta,jk} p_{\beta j} c_{\beta j} \frac{M_j}{M_i} \quad (31)$$

where \hat{F} is

$$F_{ij}^{\alpha\beta} = \delta_{\alpha\beta} [\delta_{ij} + f_\beta L_{\beta,ji}] \quad (32)$$

with $L_{\alpha,ij} = \delta_{ij} \sum_k A_{\alpha,ik} - A_{\alpha,ij} M_i/M_j$ the Laplacian matrix of the dispersal network of species α , and $f_\alpha = D_\alpha/\lambda_\alpha$. As in the single-species case, the value of f_α quantifies the colonization efficiency of species α . When f_α is greater than one, an explorer will, on average, diffuse farther through the network and reach more distant nodes from the exploration origin before attempting colonization. Conversely, when f_α is less than one, explorers will preferentially colonize patches located close to the origin.

Since \hat{F} is block-diagonal with respect to the species index, we can compute its inverse species by species, obtaining

$$(\hat{F}^{-1})_{ij}^{\alpha\beta} = \delta_{\alpha\beta} \sum_{k=1}^N \frac{(\hat{V}_\alpha)_{ik} (\hat{V}_\alpha^{-1})_{kj}}{1 + f_\alpha \omega_{\alpha k}} \quad (33)$$

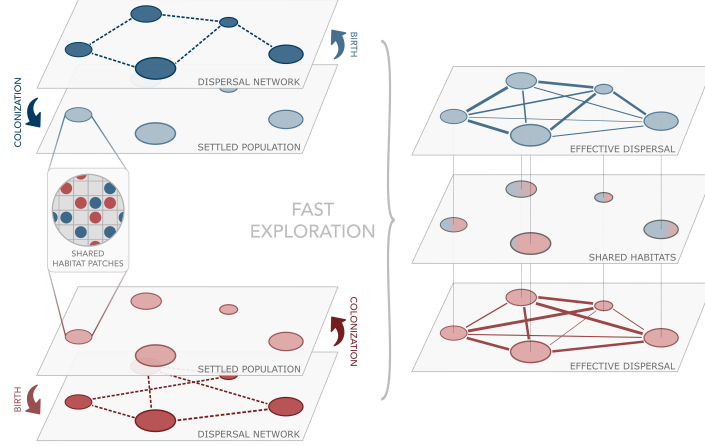


FIG. 3. Visualization of the microscopic model with multiple species competing for space or a common resource leads to an effective metacommunity model. Assuming fast exploration, time-scale separation leads to an effective kernel description (Eq. (35)) combined with the effective metacommunity equations reported in Eq. (34).

where $\omega_{\alpha k}$ is the k -th eigenvalue of \hat{L}_α , and \hat{V}_α is the matrix of its right eigenvectors. Substituting Eq. (33) into Eq. (31), and the latter into the settled density equation Eq. (29) leads to:

$$\frac{dp_{\alpha i}}{dt} = -e_{\alpha i} p_{\alpha i} + \left(1 - \sum_{\beta=1}^S p_{\beta i}\right) \sum_{j=1}^N K_{\alpha,ij} p_{\alpha j}, \quad (34)$$

where we introduced the dispersal kernel of species α

$$K_{\alpha,ji} = h_\alpha c_{\alpha i} \frac{M_j}{M_i} \sum_{k=1}^N \sum_{l=1}^N \frac{(\hat{V}_\alpha)_{ik} (\hat{V}_\alpha^{-1})_{kl}}{1 + f_\alpha \omega_{\alpha k}} A_{\alpha,jl}. \quad (35)$$

We can set $h_\alpha = \xi_\alpha / (1 + f_\alpha^{-1})$, with ξ_α representing the maximum dispersal capacity of the species. With this formulation, exploration becomes impossible when $f_\alpha \rightarrow 0$, while the kernel stays finite as $f_\alpha \rightarrow \infty$. In general, different species need not share the same dispersal network. Note that this rigorous derivation clarifies the well-known extension of classical metapopulation models to metacommunities [5].

VI. COEXISTENCE AND MONODOMINANCE IN HOMOGENEOUS AND HETEROGENEOUS HABITATS

As in the single-species case, we demonstrate how our framework can be applied to derive both analytical and numerical results on the coexistence of multiple species. We first consider a homogeneous habitat and landscape, showing that coexistence is possible only under fine-tuned conditions (a zero-measure set in parameter space). We then examine heterogeneous habitats within homogeneous landscapes (i.e., heterogeneity arising from local habitat properties) and derive analytical conditions for robust coexistence, identifying a critical level of habitat heterogeneity and its dependence on the metacommunity parameters. Finally, we show numerically that combining habitat and landscape (dispersal) heterogeneity further promotes coexistence. The proofs of all theorems and corollaries are in Section B.

A. Fragile coexistence in homogeneous habitats

We begin by examining the case of a homogeneous environment, in which local death, colonization, and birth rates are independent of the patch, and the colonization kernel is translation-invariant. As in Section III, we set $c_\alpha = 1$. In this setting, species coexistence proves to be fragile, as established by the following theorem:

Theorem 3. *Consider the following metacommunity equations:*

$$\frac{dp_{\alpha i}}{dt} = -e_\alpha p_{\alpha i} + \left(1 - \sum_{\beta=1}^S p_{\beta i}\right) \sum_{j=1}^N K_{\alpha,ij} p_{\alpha j}, \quad (36)$$

and assume that each colonization kernel \hat{K}_α is translation-invariant, and $e_\alpha > 0$ for all α . Then, the only spatially uniform stationary state in which different species can coexist is a center manifold, and it occurs for a zero-measure set in the parameter space. The center manifold is (neutrally) stable.

The previous theorem shows that coexistence is possible in homogeneous environments when the ratio e_α/z_α is equal for all species, where $z_\alpha = \sum_{j=1}^N K_{\alpha,ij}$ is the constant Fourier mode. Since z_α is proportional to the average dispersal kernel, we can interpret the ratio e_α/z_α as the inverse of fitness. Hence, we define $r_\alpha = z_\alpha/e_\alpha$ as the (average) habitat-mediated fitness, reflecting how the effective dispersal kernel arises from the interplay between habitat heterogeneity and diffusion-colonization processes.

We now consider the case where species differ in fitness. According to Theorem 3, such species cannot coexist. The following theorem establishes that the single species with the highest habitat-mediated fitness will ultimately be the only one to persist.

Theorem 4. *Consider the metacommunity equations in Theorem 3, and further assume that $e_1/z_1 < e_\alpha/z_\alpha$ for all $\alpha \neq 1$ so that the first species has the largest habitat-mediated fitness. Furthermore, assume $e_1 < z_1$, which is a necessary condition for the survival of the first species in the absence of other competing species (z_1 is the metapopulation capacity of the first species). Then, $p_\alpha^* = p_1^* \delta_{\alpha 1}$ and $p_{\beta i}^* = 0$ for $\beta \neq 1$, the state in which only the first species survives and occupies all patches uniformly is a stable fixed-point solution of the dynamics.*

Figure 4 provides a visual illustration of the two main results presented in this section. For clarity, we focus on the simplest case of two competing species. Figure 4a shows the time evolution of all habitat patches, using different colors for the two species, when $r_1 = r_2$. In this case, Theorem 3 predicts stable coexistence, with the coexistence manifold forming a center manifold. Indeed, the dynamics rapidly collapse to a spatially uniform state in which all patches of the same species have identical values, corresponding to the relaxation of spatial modes with negative eigenvalues discussed in the proof of Theorem 3. The point of the center manifold to which the system converges depends on the initial condition. Because the leading eigenvalue on the center manifold is zero, the manifold is marginally stable. A marginally stable stationary coexistence state is observed in several other ecological models [5, 57, 58].

Figure 4b shows what happens when the metacommunity is initialized with the same conditions and parameters, except for a slightly reduced habitat-mediated fitness parameter in species two. The initial transient is nearly identical to the previous case, and the system temporarily settles into the same homogeneous state. However, the homogeneous coexistence solution subsequently decays, with species two eventually going extinct and species one taking over, as prescribed by Theorem 4. Notably, the transient homogeneous coexistence state relaxes slowly and depends on the initial condition, as it lies close to the zero eigenvalue of the previous scenario.

B. Robust coexistence and niche formation in heterogeneous habitats

To understand how habitat heterogeneity shapes ecosystem diversity, we now consider the general setting in which extinction rates vary across space: $e_{\alpha i}$ depends on both species α and the habitat

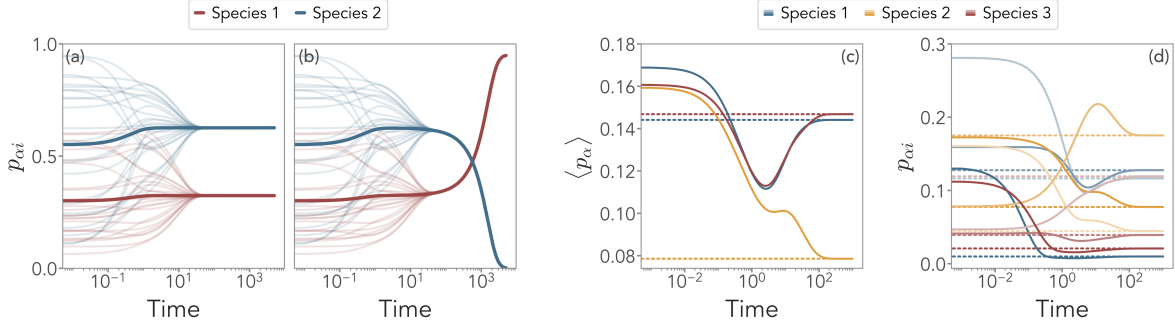


FIG. 4. (a) Fine-tuned fragile coexistence in homogeneous environments. Time evolution of $p_{\alpha i}$ (the light colored lines correspond to different patches while the dark colored lines correspond to the averages across all patches, $\langle p_{\alpha} \rangle$), $i = 1, \dots, N = 25$ and $\alpha = 1, 2 = S$ in a translationally invariant homogeneous environment (the kernel is computed from a 2D regular grid). The two species differ in exploration efficiency, with $f_1 = 1$ and $f_2 = 3$. a) Species' (average) extinction rates are chosen such that $r_1 = e_1/z_1 = e_2/z_2 = r_2 = 0.002$, with $e_1 = 0.1, e_2 = 0.15$. These conditions satisfy the hypotheses of Theorem 3, and the metacommunity dynamics converge to the center manifold. (b) Here, r_2 is 1% smaller than in (a), leading to the extinction of species 2. The transient dynamics remain close to the center manifold, which acts as a slow manifold. Since the point on the center manifold reached by the trajectory depends on the initial condition, species 2 exhibits higher abundance during the transient phase, even though it ultimately declines to zero. (c) Convergence of the dynamical evolution of the average $\langle p_{\alpha} \rangle$ to the fixed-point solution, with three species (dotted lines) given by Eq. (44) for the kernel given by Eq. (38). (d) Same, but for the average abundance of each species in each patch, given by Eq. (41). Here, $r_{\alpha i}$ were chosen from a lognormal distribution with mean 1.5 and standard deviation equal to 2.

patch i . The starting point is the full metapopulation model,

$$\dot{p}_{\alpha i} = -e_{\alpha i} p_{\alpha i} + \left(1 - \sum_{\beta=1}^S p_{\beta i}\right) \sum_{j=1}^N K_{\alpha,ij} p_{\alpha j}. \quad (37)$$

A direct substitution shows that, in this more general scenario, the spatially uniform coexistence solution discussed in the previous section is no longer a stationary state of Eq. (37).

To derive explicit and minimal analytical conditions for coexistence, we first examine the mean-field limit, in which dispersal depends only on the species and not on specific patches. To ensure a meaningful limit for $N \rightarrow \infty$, we let the kernel elements scale as

$$K_{\alpha,ij} = \frac{K_{\alpha}}{N}. \quad (38)$$

which corresponds to a fully connected network in Eq. (35). We define the spatial average abundance as

$$\frac{1}{N} \sum_j p_{\alpha j} = \langle p_{\alpha} \rangle, \quad (39)$$

and the free space in patch i as

$$Q_i = 1 - \sum_{\beta=1}^S p_{\beta i}. \quad (40)$$

We can now write the following equation for the steady-state solution of Eq. (37):

$$p_{\alpha i}^* = r_{\alpha i} Q_i \langle p_{\alpha} \rangle, \quad (41)$$

where Q_i is implicitly determined by all $p_{\alpha i}^*$, and we define

$$r_{\alpha i} = \frac{K_\alpha}{e_{\alpha i}} \quad (42)$$

as the *local* habitat-mediated fitness of species α in patch i , as $r_{\alpha i}$ quantifies the balance between colonization and extinction within each patch, and results from the interplay of species traits with local landscape properties. Using Eq. (40), Eq. (41), averaging over patches yields

$$Q_i = \left(1 + \sum_{\alpha} r_{\alpha i} \langle p_{\alpha}^* \rangle \right)^{-1}. \quad (43)$$

and, using again Eq. (41), we obtain the self-consistency equation:

$$\langle p_{\alpha}^* \rangle = \frac{\langle p_{\alpha}^* \rangle}{N} \sum_{i=1}^N r_{\alpha i} \left(1 + \sum_{\beta=1}^S r_{\beta i} \langle p_{\beta}^* \rangle \right)^{-1}. \quad (44)$$

For any fixed choice of $r_{\alpha i}$, Eq. (44) can be solved numerically for $\langle \vec{p} \rangle$, which in turn allows the reconstruction of the full solution $p_{\alpha i} \forall \alpha, i$ by exploiting Eq. (41). Figure 4c shows an example of how $\langle p_{\alpha} \rangle(t)$ (solid lines) evolves toward the self-consistent solution (dotted lines) of Eq. (44), while Figure 4d shows the same for individual patches, Eq. (41).

To make analytical progress, we now treat these fitness values as quenched random variables. For simplicity, we drop the asterisk from now on, i.e. $p_{\alpha i}^* \equiv p_{\alpha i}$. We focus on coexistence solutions, defined by

$$\langle p_{\alpha} \rangle > 0 \quad \forall \alpha = 1, \dots, S. \quad (45)$$

In the limit $N \rightarrow \infty$, Eq. (44) becomes the following self-consistency relations for the mean densities $\langle p_{\alpha} \rangle$

$$1 = \frac{1}{N} \sum_{i=1}^N r_{\alpha i} \left(1 + \sum_{\beta=1}^S r_{\beta i} \langle p_{\beta}^* \rangle \right)^{-1} = \left\langle \frac{r_{\alpha}}{1 + \sum_{\beta=1}^S r_{\beta} \langle p_{\beta}^* \rangle} \right\rangle. \quad (46)$$

Next, we assume that for each species α , the random variables $r_{\alpha i}$ are drawn independently from a distribution $P_r(r|\vec{\zeta}_{\alpha})$ whose parameters $\vec{\zeta}_{\alpha}$ may differ across species. We now introduce the Laplace transform of this distribution as

$$W_{\alpha}(\omega) = \int_0^{\infty} dr P_r(r|\vec{\zeta}_{\alpha}) e^{-r\omega}. \quad (47)$$

Using this definition, together with the identity valid for $z > 0$,

$$\frac{1}{z} = \int_0^{\infty} d\lambda e^{-z\lambda}, \quad (48)$$

we derive from Eq. (46) the following implicit equations for the vector $\langle \vec{p} \rangle$

$$1 = \int_0^{\infty} d\lambda e^{-\lambda} \left(-\frac{\partial}{\partial \omega} \ln W_{\alpha}(\omega) \right)_{\omega=\lambda \langle p_{\alpha}^* \rangle} \prod_{\beta} W_{\beta}(\lambda \langle p_{\beta}^* \rangle). \quad (49)$$

C. Critical habitat heterogeneity for coexistence

We now consider the case that S is large, and perform the rescaling $x_\beta = S\langle p_\beta \rangle$ and $\lambda = Sz$. The self-consistent equations for the rescaled mean abundances become

$$1 = S \int_0^\infty dz e^{-S\bar{F}(z, \vec{x})} \left(-\frac{W'_\alpha(zx_\alpha)}{W_\alpha(zx_\alpha)} \right) \quad (50)$$

where

$$\bar{F}(z, \vec{x}) = z - \frac{1}{S} \sum_{\beta=1}^S \ln W_\beta(z \cdot x_\beta). \quad (51)$$

Taking the derivative of Eq. (51) with respect to z shows that $\partial_z \bar{F}(z, \vec{x}) > 0$, which implies that its minimum occurs at $z = 0$. Thus, we expect the integral to be dominated by the value around $z = 0$ when S is large. We can perform a Taylor expansion of Eq. (51):

$$\bar{F}(z, \vec{x}) = z \left(1 + \frac{1}{S} \sum_{\beta} x_\beta \langle r_\beta \rangle \right) - \frac{z^2}{2} \frac{1}{S} \sum_{\beta} v_\beta^2 x_\beta^2 + \mathcal{O}(z^3) \quad (52)$$

where $v_\beta^2 = \langle r_\beta^2 \rangle - \langle r_\beta \rangle^2$ denotes the variance of $P_r(r|\zeta_\alpha)$. We now introduce the following two quantities, defined as averages over species,

$$\overline{x \langle r \rangle} = \lim_{S \rightarrow \infty} \frac{1}{S} \sum_{\beta=1}^S x_\beta \langle r_\beta \rangle; \quad \overline{x^2 v^2} = \lim_{S \rightarrow \infty} \frac{1}{S} \sum_{\beta=1}^S x_\beta^2 v_\beta^2. \quad (53)$$

Inserting the last three equations into Eq. (50), we obtain

$$1 = \frac{\langle r_\alpha \rangle}{1 + \overline{x \langle r \rangle}} + \frac{1}{S} \frac{1}{(1 + \overline{x \langle r \rangle})^2} \left[\frac{\langle r_\alpha \rangle}{1 + \overline{x \langle r \rangle}} \overline{x^2 v^2} - x_\alpha v_\alpha^2 \right] + \mathcal{O}\left(\frac{1}{S^2}\right). \quad (54)$$

Equation (54) implies that for coexistence to be possible $\langle r_\alpha \rangle$ must scale as follows with respect to $1/S$:

$$\langle r_\alpha \rangle = R + \frac{\Delta_\alpha}{S} + \mathcal{O}\left(\frac{1}{S^2}\right), \quad (55)$$

where R and Δ_α are functions of ζ_α . In particular, if R is the average or ‘‘baseline’’ fitness of the metacommunity, each species’ deviation from such baseline must scale as $1/S$, and can hence be indicated as Δ_α/S . Next, we plug Eq. (55) into Eq. (54) and obtain

$$1 + \overline{x \langle r \rangle} = R + \frac{1}{S} \left[\Delta_\alpha + \frac{1}{1 + \overline{x \langle r \rangle}} \left(\frac{R}{1 + \overline{x \langle r \rangle}} \overline{x^2 v^2} - x_\alpha v_\alpha^2 \right) \right] + \mathcal{O}\left(\frac{1}{S^2}\right) \quad (56)$$

$$= R + \frac{1}{S} \left[\Delta_\alpha + \frac{1}{R} \left(\overline{x^2 v^2} - x_\alpha v_\alpha^2 \right) \right] + \mathcal{O}\left(\frac{1}{S^2}\right). \quad (57)$$

We now observe that the right-hand side cannot depend on the species index. Therefore, the rescaled stationary population $x_\alpha = S \langle p_\alpha \rangle$ must be

$$x_\alpha = \frac{\Delta_\alpha - H}{v_\alpha^2} R + \mathcal{O}\left(\frac{1}{S}\right), \quad (58)$$

where H is a constant to be determined. Equation (56) implies that

$$R - 1 = \overline{x \langle r \rangle} = \frac{R}{S} \sum_{\alpha} x_{\alpha} = \frac{R^2}{S} \sum_{\alpha} \frac{\Delta_{\alpha} - H}{v_{\alpha}^2}, \quad (59)$$

at the leading order in $1/S$. We can now solve for H ;

$$H = \left(\frac{1}{S} \sum_{\alpha} \frac{1}{v_{\alpha}^2} \right)^{-1} \left[\frac{1}{S} \sum_{\alpha} \frac{\Delta_{\alpha}}{v_{\alpha}^2} - \frac{R-1}{R^2} \right] = \left(\frac{1}{v^2} \right)^{-1} \left[\left(\frac{\bar{\Delta}}{v^2} \right) - \frac{R-1}{R^2} \right], \quad (60)$$

where we recall that $(\bar{\cdot}) := \frac{1}{S} \sum_{\alpha} (\cdot)$ indicates an average over species. Survival of all species occurs if

$$\Delta_{\alpha} > H \quad \forall \alpha. \quad (61)$$

We can simplify this coexistence condition assuming that $v_{\alpha}^2 = v^2$, that is, the disorder variance is the same for all species. In this case, the threshold for survival H takes the simple form:

$$\Delta_{\alpha} > H = \bar{\Delta} - v^2 \frac{R-1}{R^2}. \quad (62)$$

where the overbar indicates the usual average over species

$$\bar{\Delta} = \frac{1}{S} \sum_{\alpha} \Delta_{\alpha}. \quad (63)$$

From Eq. (59) and Eq. (62) it follows that $R > 1$ and

$$\min_{\alpha} \Delta_{\alpha} > \bar{\Delta} - v^2 \frac{R-1}{R^2}. \quad (64)$$

We can rewrite this last condition as follows

$$v^2 > v_c^2 := \gamma_{\Delta} \frac{R^2}{R-1}, \quad \gamma_{\Delta} = \bar{\Delta} - \min \Delta_{\alpha}, \quad (65)$$

which defines a critical value for the disorder variance, v_c . The quantity γ_{Δ} is a measure of how heterogeneous the species' average fitnesses are. Hence, Eq. (65) predicts that a stronger habitat disorder is needed for the coexistence of species with larger differences in their mean fitness. On the contrary, if they are all equal, i.e. $\langle r \rangle = R$, then

$$\gamma_{\Delta} = 0 \implies x_{\alpha} = \frac{R-1}{R}, \quad (66)$$

so that $R > 1$ is the only condition determining either full coexistence or the extinction of all species.

Now, we show how these analytical predictions compare to numerical simulations. In Figure 5a, we choose a log-normal distribution for the local habitat-mediated fitness distribution $P_r(r)$ and show the fraction of coexisting species in the (R, v^2) -coordinate space for a fixed Δ_{α} . The black vertical line represents the first (co)existence condition $R > 1$. Indeed, we observe that when $R < 1$, no species survives. The second black line corresponds to the critical disorder variance boundary Eq. (65). The transition from partial to full coexistence is smooth here because S, N are finite, but becomes sharp in the limit $N, S \rightarrow \infty$. Coexistence of all species indeed requires sufficiently large habitat heterogeneity (i.e., large enough v^2). Interestingly, the critical variance increases as a function of R , as Eq. (65) makes clear. The intuitive interpretation is that, in this case, all species have high baseline fitness, which effectively increases competition. Hence, intermediate values of R are optimal for coexistence under fixed habitat heterogeneity. This observation suggests that coexistence does not correspond to

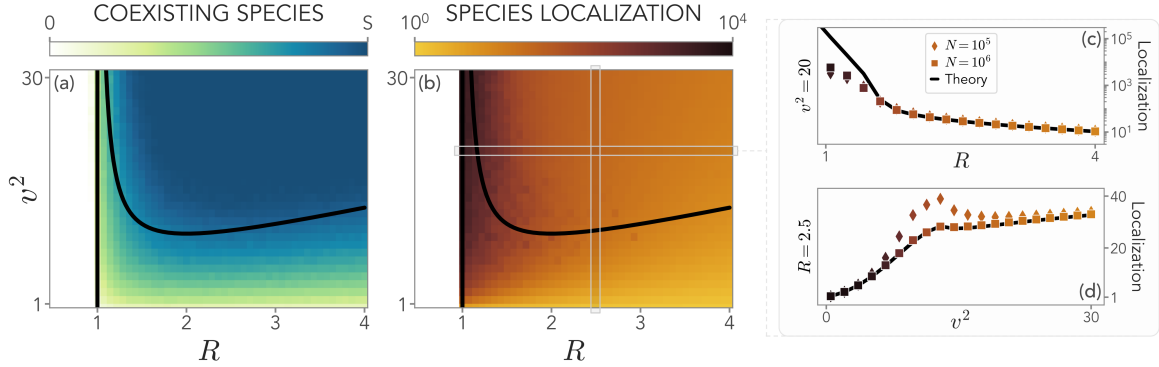


FIG. 5. Analytical phase diagram of coexistence regions with mean-field dispersion in heterogeneous habitats. (a) Fraction of coexisting species as a function of the baseline metacommunity fitness R and habitat disorder variance v^2 . (b) Species localization as a function of the same parameters shows increased localization in the coexisting phase and a strong increase near the global extinction boundary $R = 1$. (c) Horizontal slice of panel (b) showing localization as a function of R , at a fixed disorder value. A strong increase in the localization near the extinction boundary is observed. (d) Vertical slice of panel (b), localization as a function of the disorder variance for a fixed R , which shows the increase of localization when transitioning from monodominance to coexistence, as an indication of niche formation. Numerical simulations are obtained using a log-normal distribution for the disorder. Here, Δ_α is evenly spaced between $\pm 5/2$, so that $\gamma_\Delta = 2.5$. The theory is computed from numerical integration of Eq. (71). An expansion for large S only gives an accurate prediction for very large S . Adapted from ref. [47].

evenly spread species densities, but is rather associated with some kind of spatial localization. To quantify localization explicitly, we use the following measure

$$\text{Loc}_\alpha \equiv \frac{\frac{1}{N} \sum_i p_{\alpha i}^4}{\left(\frac{1}{N} \sum_i p_{\alpha i}^2 \right)^2} = \frac{\langle p_\alpha^4 \rangle}{\langle p_\alpha^2 \rangle^2}, \quad (67)$$

which is related to the inverse participation ratio. If the distribution of species α is uniform within a subset E covering $K \leq N$ patches, then $p_{\alpha i} \approx \mathbf{1}_E(i)p^*$, where $\mathbf{1}_E$ is the indicator function of set E . Substituting into Eq. (67) we obtain

$$\text{Loc}_\alpha = \frac{N}{K}. \quad (68)$$

Hence, when the species occupies all patches evenly $\text{Loc}_\alpha \approx 1$, and $\text{Loc}_\alpha \approx N$ when it is present only within a single patch. To find an analytical expression for the localization, we need to compute the moments of p_α . For this purpose, we combine Eq. (41) with Eq. (43), yielding

$$p_{\alpha i} = \frac{\langle p_\alpha \rangle r_{\alpha i}}{1 + \sum_{\beta=1}^S r_{\beta i} \langle p_\beta \rangle}, \quad (69)$$

which provides a link between the moments r_α and those of p_α . Next, by employing the following identity, which holds for $z > 0$,

$$\frac{1}{z^m} = \frac{1}{\Gamma[m]} \int_0^\infty d\lambda \lambda^{m-1} e^{-z\lambda}, \quad (70)$$

we can proceed as in the previous section to obtain

$$\langle p_\alpha^m \rangle = \frac{x_\alpha^m}{\Gamma(m)} \int_0^\infty dz z^{m-1} e^{-S\bar{F}(z,x)} \frac{W^{(m)}(zx_\alpha)}{W(zx_\alpha)}, \quad (71)$$

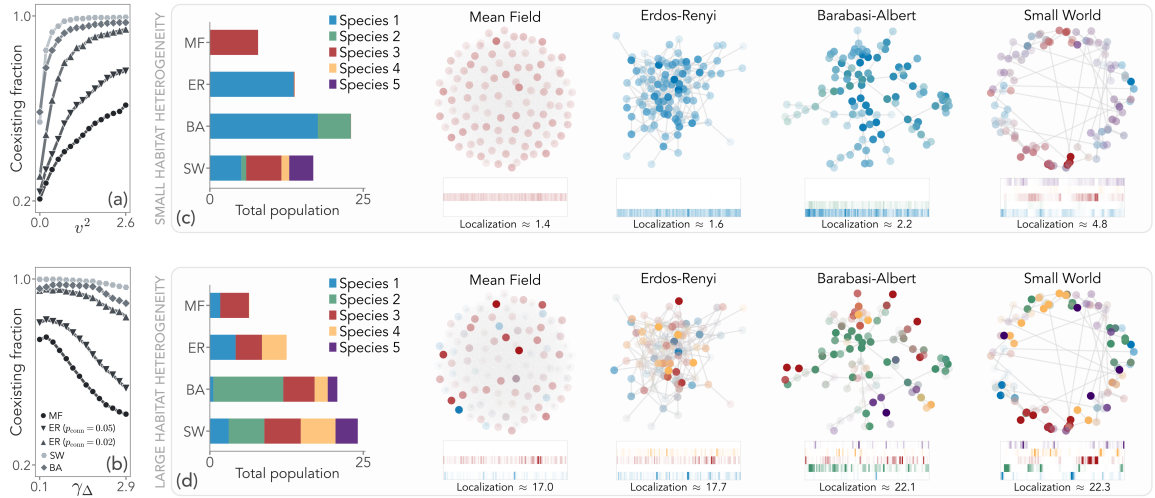


FIG. 6. Fraction of coexisting species as a function of habitat disorder (a) and species heterogeneity (b) for different network topologies: Erdős-Rényi(ER) with two different sparsity levels, small-world (SW), and Barabási-Albert (BA), compared to the mean-field (MF) kernel (see legend in panel b inset). In panel (a), $R = 2$, $\gamma_\Delta = 1$, $S = 5$, and $N = 100$. In panel (b), the same parameters are used with $v^2 = 3$. Due to finite-size effects, full coexistence is not observed in the mean-field case, even when γ_Δ is small. (c-d) At sufficiently high habitat heterogeneity, dispersal networks support a larger number of coexisting species and a higher total population than MF at constant average habitat-mediated fitness. Color transparency indicates the population density in each patch. Here, we set $\gamma_\Delta = 0$. Parts of figure adapted from [47]

where $x_\alpha = \langle p_\alpha \rangle S$, as above, and $W_\alpha(\omega)$ was defined in Eq. (47).

In Figure 5b, we plot the localization, averaged over species, in the same (R, v^2) coordinate space, while Figure 5c-d show a horizontal and a vertical slice, respectively. The general behavior of the localization confirms the intuition that the coexisting phase is characterized by increased localization and, hence, reflects spatial niche formation. To show more explicitly that localization increases markedly as the habitat disorder v^2 grows and the system transitions from the monodominance to the coexistence phase, we consider a vertical cut of the phase space (Figure 5d), where simulation data are compared to the theory for two values of the system size N . Another notable observation from Figure 5b is that the localization undergoes a sharp increase as the global extinction boundary $R > 1$ is approached. The ecological interpretation here is that near this threshold, species maximize their spatial segregation, as any competition could push them below the extinction threshold.

D. Landscape structure fosters coexistence

The mean-field kernel studied in the previous subsection corresponds to an all-to-all dispersal network. We can now compare the qualitative picture of the mean-field analytics to the more general scenario of a kernel obtained from a generic network using Eq. (35). More specifically, we contrast the mean-field (MF) results with three prototypical networks: Erdős-Rényi(ER) networks with two different average connection probabilities, thus illustrating the effects of network sparsity; Barabási-Albert (BA) networks, characterized by the presence of highly connected nodes; and small-world (SW) networks, which feature a high clustering coefficient. To perform this comparison in practice, in analogy to Eq. (42), we can define the local species fitness as $r_{\alpha i} = N \langle K_\alpha \rangle / e_{\alpha i}$, where $N \langle K_\alpha \rangle \equiv \sum_i K_{\alpha i}$, which reduces to Eq. (38) in the mean field case. Then, we consider a realization of the quenched disorder $r_{\alpha i}$ and, for each species α , compute the kernel elements $K_{\alpha,ij}$ and its average $\langle K_\alpha \rangle$, from which we obtain the extinction rates as $e_{\alpha i} = N \langle K_\alpha \rangle / r_{\alpha i}$. In this way, $\langle r_\alpha \rangle$ does not depend on the specific network, ensuring comparable survivability for a given species α across different landscape topologies.

Figure 6a shows that the main finding remains qualitatively unchanged: the fraction of coexisting species increases with habitat heterogeneity v^2 across all networks, as in the MF case. However, the structure of the dispersal kernel quantitatively shifts the transition to coexistence, making it easier to achieve. ER networks support a larger fraction of coexisting species at a given disorder strength. Interestingly, coexistence is further enhanced as sparsity increases. At the same fixed level of sparsity, coexistence is also enhanced in BA networks and in a SW topology (Figure 6a).

We can also observe our key result on the critical disorder strength Eq. (65) from a different perspective: at a fixed habitat disorder strength v^2 and baseline fitness of the community, there is a maximum level of species heterogeneity that can be supported. Indeed, Figure 6b shows that the fraction of coexisting species decreases with γ_Δ across all kernel types.

Finally, we visualize the spatial niche formation and the qualitative effect of kernel structure in Figure 6c. For simplicity, we consider the “neutral” case, in which $\gamma_\Delta = 0$ and the competing species have equal average habitat-mediated fitness. For the same realization of $r_{\alpha i}$, structured landscapes support a larger number of species as well as a higher total population (Figure 6c). Interestingly, although all species in this example have the same average fitness, the interplay between spatial heterogeneity and the dispersal network structure determines which species survive where, leading to uneven population distributions (Figure 6c). For instance, species two (green) has the largest population in the BA network because it happens to have higher fitness in the major network hub. The clusters in the SW network appear to strike a balance between segregation, which buffers competition, and colonization boost, which increases population. Hence, landscape structure plays a key role in shaping both species survival and their spatial distribution.

VII. OUTLOOK - INCORPORATING GENERAL ECOLOGICAL PROCESSES INTO DISPERSAL DYNAMICS

Until now, we focused on how species survival and coexistence are shaped by the interplay between dispersal across landscapes – in different scenarios of spatial homogeneity and heterogeneity – and competitive interactions with other species. We specifically examined competitive interactions, given their fundamental and widespread role in driving species exclusion from a metacommunity. However, a broad spectrum of ecological interactions can influence species survival within a metacommunity and affect overall ecosystem biodiversity. These processes include density-dependent birth and death rates, trophic interactions, or facilitation. Below, we give a few examples of how such processes can be incorporated into the present framework, focusing on the deterministic rate-based perspective.

One first extension is to allow for settled individuals to give birth directly, without going through the generation of explorers. In the case of plants, this could represent vegetative propagation, which consists of new plants growing from vegetative parts such as roots, stems, or leaves. In this scenario, we add the following reaction



This reaction does not affect the explorer dynamics. In the fast-exploration limit discussed above, the effective kernel Eq. (35) also remains unchanged, and the metacommunity rate equations become

$$\dot{p}_{\alpha i} = -e_{\alpha i}p_{\alpha i} + b_{\alpha i} \left(1 - \sum_{\beta=1}^S p_{\beta i} \right) p_{\alpha i} + \left(1 - \sum_{\beta=1}^S p_{\beta i} \right) \sum_{j=1}^N K_{\alpha,ij} p_{\alpha j} \quad (73)$$

$$= -(e_{\alpha i} - b_{\alpha i})p_{\alpha i} - \sum_{\beta=1}^S b_{\alpha i}p_{\alpha i}p_{\beta i} + \left(1 - \sum_{\beta=1}^S p_{\beta i} \right) \sum_{j=1}^N K_{\alpha,ij} p_{\alpha j}, \quad (74)$$

which makes it clear that the addition of this reaction contributes a logistic term, which can be split into a linear growth and a quadratic self-limitation term that depends on the local abundance of all species.

Another ecological reaction leading to a negative quadratic term is the following:



which models generic competitive interference between different species (if $\alpha \neq \beta$) or an intra-species self-limitation term (if $\alpha = \beta$). Equation (75) models the death of a settled individual of species β caused by the presence of a settled individual of species α . Here, for notational simplicity, we assume that the competitive interference matrix $\Gamma_{\alpha\beta}$ does not depend on the patch index. This reaction leads to the following rate dynamics:

$$\dot{p}_{\alpha i} = -e_{\alpha i} p_{\alpha i} - \sum_{\beta=1}^S \Gamma_{\alpha\beta} p_{\alpha i} p_{\beta i} + \left(1 - \sum_{\beta=1}^S p_{\beta i}\right) \sum_{j=1}^N K_{\alpha,ij} p_{\alpha j}, \quad (76)$$

which shows that this process also leads to a quadratic loss term. An equivalent rate description can be obtained by assuming that the death rate of settled individuals includes a density-dependent component:



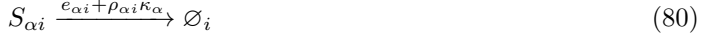
A quadratic self-interaction term (i.e. with only species-diagonal elements) can also arise as a simplified representation of the Janzen-Connell hypothesis [59], that is, assuming that each species is affected by specific pathogens. These pathogens undergo logistic growth, tied to the abundance of the infected species:

$$\dot{\rho}_{\alpha i} = \rho_{\alpha i} \left(p_{\alpha i} - \frac{\Gamma_{\alpha\alpha}}{\kappa_{\alpha}} \rho_{\alpha i} \right), \quad (78)$$

where $\rho_{\alpha i}$ is the normalized density of pathogens. Assuming that the infection and recovery dynamics of the pathogen cycle are fast relative to the birth/death timescales of the settled population, we obtain from Eq. (78):

$$p_{\alpha i} = \frac{\Gamma_{\alpha\alpha}}{\kappa_{\alpha}} \rho_{\alpha i}. \quad (79)$$

Introducing a pathogen-dependent death rate for species α :



ultimately leads to:

$$\dot{p}_{\alpha i} = -e_{\alpha i} p_{\alpha i} - \Gamma_{\alpha\alpha} p_{\alpha i}^2 + \left(1 - \sum_{\beta=1}^S p_{\beta i}\right) \sum_{j=1}^N K_{\alpha,ij} p_{\alpha j}. \quad (81)$$

Local interactions could also cause a species to be positively influenced by the presence of another, as in the case of facilitation or trophic interactions. In this scenario, the effective metacommunity description would be

$$\dot{p}_{\alpha i} = -e_{\alpha i} p_{\alpha i} + \sum_{\beta=1}^S \Phi_{\alpha\beta} p_{\alpha i} p_{\beta i} + \left(1 - \sum_{\beta=1}^S p_{\beta i}\right) \sum_{j=1}^N K_{\alpha,ij} p_{\alpha j}, \quad (82)$$

in which the interaction matrix $\Phi_{\alpha\beta}$ can have positive, negative, or zero entries according to the type of local interaction. To ensure that the local density does not exceed unity, the sign and magnitude of the Φ matrix entries need to obey specific constraints. For instance, the reaction



which could be a simple model of a predator-prey interaction, implies that $\Phi_{\alpha\beta} = -\Phi_{\beta\alpha}$. More generally, requiring that, whenever $\Phi_{\alpha\beta} > 0$, the corresponding entry $\Phi_{\beta\alpha}$ is negative and at least as large in magnitude is sufficient to guarantee that the settled densities remain bounded by one.

VIII. CONCLUDING REMARKS

This work refines and unifies recent developments in the mechanistic theory of metacommunity dynamics [42, 47, 48], providing a systematic framework to derive effective models that explicitly link microscopic ecological processes, landscape structure, and emergent community patterns. By starting from a microscopic description and coarse-graining to effective equations, we have shown how a wide range of ecological processes – dispersal, colonization, extinction, stochasticity, and interspecific interactions – can be incorporated within a single, analytically tractable formalism.

In the single-species case, the structure of the dispersal network and the heterogeneity of local habitats jointly determine species persistence. In particular, Theorem 1 demonstrates how dispersal couples local habitat variations into a global property that governs persistence. This formal result aligns with empirical observations suggesting that local habitat heterogeneity can impact the global population status through dispersal [60–62].

In the stochastic regime, we have connected extinction-time statistics and finite-size scaling exponents to underlying ecological parameters, revealing a universal scaling structure for noise-driven extinction. Future investigations could explore how persistence-time distributions and associated statistics change with variation in the microscopic reactions and/or dispersal-network properties, for instance by applying tools from response theory and stochastic inference in systems with absorbing boundary conditions [63–69].

Extending the framework to multiple interacting species, we find that space effectively acts as the limiting resource: in homogeneous environments, competitive exclusion leads to monodominance except for a fine-tuned neutral manifold, in which the homogeneous coexistence state depends on the initial condition. Interestingly, we observed that a small amount of disorder does not support biodiversity, and we showed that a critical level of habitat heterogeneity is needed to create stable ecological niches and enable coexistence. This critical transition, smoothed for finite systems, might be a way of reconciling contrasting reports of the effect of habitat heterogeneity on species coexistence [70–76].

The generality of the microscopic construction makes it possible to extend the present framework to other ecological processes. Future efforts should investigate the effect of the additional terms on species coexistence. Quadratic self-limitation terms are expected to introduce a self-regulation that buffers interspecific competition and could stabilize coexistence [77]. Incorporating predator-prey or trophic interactions could likewise alter the coexistence conditions [78] and possibly cause chaotic population dynamics [15, 79–81], offering a route to explore the emergence of non-equilibrium behavior in structured landscapes beyond the fixed-point equilibria observed here.

A key challenge for future work lies in connecting theoretical parameters to empirical data. While the dispersal network might be inferred from spatial connectivity or movement data, detailed local rates and interaction parameters may be difficult to estimate. Recent work explored a promising approach assuming a suitable random kernel and inferring distribution parameters from empirical abundances in data-rich communities [82]. Altogether, this framework establishes a versatile and extensible foundation for studying spatially structured ecosystems through the lens of non-equilibrium statistical mechanics, enabling both theoretical advances and data-driven applications.

- [1] S. A. Levin, The problem of pattern and scale in ecology, *Ecology* **73**, 1943 (1992).
- [2] D. Tilman, Competition and biodiversity in spatially structured habitats, *Ecology* **75**, 2 (1994).
- [3] S. A. Levin, Multiple scales and the maintenance of biodiversity, *Ecosystems* **3**, 498 (2000).
- [4] I. Hanski and O. Ovaskainen, The metapopulation capacity of a fragmented landscape., *Nature* **404**, 755 (2000).
- [5] N. Mouquet and M. Loreau, Coexistence in metacommunities: the regional similarity hypothesis, *The American Naturalist* **159**, 420 (2002).
- [6] J. Chave, H. Muller-Landau, and S. Levin, Comparing classical community models: Theoretical consequences for patterns of diversity, *American Naturalist* **159**, 1 (2002).

- [7] M. Di Musciano, V. Di Cecco, F. Bartolucci, F. Conti, A. R. Frattaroli, and L. Di Martino, Dispersal ability of threatened species affects future distributions, *Plant Ecology* **221**, 265 (2020).
- [8] M. F. Diniz, S. A. Cushman, R. B. Machado, and P. De Marco Junior, Landscape connectivity modeling from the perspective of animal dispersal, *Landscape Ecology* **35**, 41 (2020).
- [9] S.-C. Chen, P. Poschlod, A. Antonelli, U. Liu, and J. B. Dickie, Trade-off between seed dispersal in space and time, *Ecology Letters* **23**, 1635 (2020).
- [10] L. H. Loke and R. A. Chisholm, Unveiling the transition from niche to dispersal assembly in ecology, *Nature* **618**, 537 (2023).
- [11] L. Marrec, I. Lamberti, and A.-F. Bitbol, Toward a universal model for spatially structured populations, *Physical Review Letters* **127**, 218102 (2021).
- [12] A. Abbara and A.-F. Bitbol, Frequent asymmetric migrations suppress natural selection in spatially structured populations, *PNAS Nexus* **2**, pgad392 (2023).
- [13] M. K. Denk-Lobnig and K. B. Wood, Spatial population dynamics of bacterial colonies with social antibiotic resistance, *Proceedings of the National Academy of Sciences* **122**, e2417065122 (2025).
- [14] S. Allesina and S. Tang, Stability criteria for complex ecosystems, *Nature* **483**, 205 (2012).
- [15] F. Roy, M. Barbier, G. Biroli, and G. Bunin, Complex interactions can create persistent fluctuations in high-diversity ecosystems, *PLoS computational biology* **16**, e1007827 (2020).
- [16] A. Altieri, F. Roy, C. Cammarota, and G. Biroli, Properties of equilibria and glassy phases of the random lotka-volterra model with demographic noise, *Physical Review Letters* **126**, 258301 (2021).
- [17] J. W. Baron, T. J. Jewell, C. Ryder, and T. Galla, Breakdown of random-matrix universality in persistent lotka-volterra communities, *Physical Review Letters* **130**, 137401 (2023).
- [18] L. Poley, J. W. Baron, and T. Galla, Generalized lotka-volterra model with hierarchical interactions, *Physical Review E: Statistical Physics, Plasmas, Fluids, and Related Interdisciplinary Topics* **107**, 024313 (2023).
- [19] I. A. Hatton, O. Mazzarisi, A. Altieri, and M. Smerlak, Diversity begets stability: Sublinear growth and competitive coexistence across ecosystems, *Science* **383**, eadg8488 (2024).
- [20] S. Díaz, J. Fargione, F. S. Chapin, and D. Tilman, Biodiversity loss threatens human well-being, *PLoS Biology* **4**, e277 (2006).
- [21] D. Tilman, M. Clark, D. R. Williams, K. Kimmel, S. Polasky, and C. Packer, Future threats to biodiversity and pathways to their prevention, *Nature* **546**, 73 (2017).
- [22] F. Isbell, A. Gonzalez, M. Loreau, J. Cowles, S. Díaz, A. Hector, G. M. Mace, D. A. Wardle, M. I. O'Connor, J. E. Duffy, *et al.*, Linking the influence and dependence of people on biodiversity across scales, *Nature* **546**, 65 (2017).
- [23] J. Bascompte and R. V. Solé, Habitat fragmentation and extinction thresholds in spatially explicit models, *Journal of Animal Ecology* , 465 (1996).
- [24] I. Hanski, *Metapopulation Ecology* (Oxford Univ. Press, Oxford, 1999).
- [25] T. Reichenbach, M. Mobilia, and E. Frey, Mobility promotes and jeopardizes biodiversity in rock–paper–scissors games, *Nature* **448**, 1046 (2007).
- [26] L. J. Gilarranz and J. Bascompte, Spatial network structure and metapopulation persistence, *Journal of Theoretical Biology* **297**, 11 (2012).
- [27] J. W. Baron and T. Galla, Dispersal-induced instability in complex ecosystems, *Nature communications* **11**, 6032 (2020).
- [28] M. Tejo, C. Quiñinao, R. Rebollo, and P. A. Marquet, Coexistence, dispersal and spatial structure in metacommunities: a stochastic model approach, *Theoretical Ecology* **14**, 279 (2021).
- [29] F. Wu, Y. Ha, A. Weiss, M. Wang, J. Letourneau, S. Wang, N. Luo, S. Huang, C. T. Lee, L. A. David, and L. You, Modulation of microbial community dynamics by spatial partitioning, *Nature Chemical Biology* **18**, 394 (2022).
- [30] E. E. Holmes, M. A. Lewis, J. E. Banks, and R. R. Veit, Partial differential equations in ecology: Spatial interactions and population dynamics, *Ecology* **75**, 17 (1994).
- [31] R. Cantrell and C. Cosner, Diffusion models for population dynamics incorporating individual behavior at boundaries: Applications to refuge design, *Theoretical Population Biology* **55**, 189 (1999).
- [32] M. A. Leibold, M. Holyoak, N. Mouquet, P. Amarasekare, J. M. Chase, M. F. Hoopes, R. D. Holt, J. B. Shurin, R. Law, D. Tilman, *et al.*, The metacommunity concept: a framework for multi-scale community ecology, *Ecology letters* **7**, 601 (2004).
- [33] I. Hanski, Metapopulation dynamics, *Nature* **396**, 41 (1998).
- [34] R. M. May, Will a large complex system be stable?, *Nature* **238**, 413 (1972).
- [35] S. Allesina and S. Tang, The stability–complexity relationship at age 40: a random matrix perspective, *Population Ecology* **57**, 63 (2015).
- [36] G. Biroli, G. Bunin, and C. Cammarota, Marginally stable equilibria in critical ecosystems, *New Journal*

of Physics **20**, 083051 (2018).

[37] S. Azaele, S. Suweis, J. Grilli, I. Volkov, J. R. Banavar, and A. Maritan, Statistical mechanics of ecological systems: Neutral theory and beyond, *Reviews of Modern Physics* **88**, 035003 (2016).

[38] G. Bunin, Ecological communities with lotka-volterra dynamics, *Phys. Rev. E* **95**, 042414 (2017).

[39] T. Galla, Dynamically evolved community size and stability of random lotka-volterra ecosystems(a), *Europhysics Letters* **123**, 48004 (2018).

[40] S. Suweis, F. Ferraro, C. Grilletta, S. Azaele, and A. Maritan, Generalized lotka-volterra systems with time correlated stochastic interactions, *Phys. Rev. Lett.* **133**, 167101 (2024).

[41] I. Akjouj, M. Barbier, M. Clenet, W. Hachem, M. Maïda, F. Massol, J. Najim, and V. C. Tran, Complex systems in ecology: a guided tour with large lotka–volterra models and random matrices, *Proceedings of the Royal Society A: Mathematical, Physical and Engineering Sciences* **480**, <https://doi.org/10.1098/rspa.2023.0284> (2024).

[42] G. Nicoletti, P. Padmanabha, S. Azaele, S. Suweis, A. Rinaldo, and A. Maritan, Emergent encoding of dispersal network topologies in spatial metapopulation models, *Proc. Natl. Acad. Sci.* **120**, e2311548120 (2023).

[43] M. D. Holland and A. Hastings, Strong effect of dispersal network structure on ecological dynamics, *Nature* **456**, 792 (2008).

[44] F. Guichard and T. C. Gouhier, Non-equilibrium spatial dynamics of ecosystems, *Mathematical Biosciences* **255**, 1 (2014).

[45] J. Denk and O. Hallatschek, Self-consistent dispersal puts tight constraints on the spatiotemporal organization of species-rich metacommunities, *Proceedings of the National Academy of Sciences* **119**, e2200390119 (2022).

[46] J. Nauta and M. De Domenico, Topological conditions drive stability in meta-ecosystems, *Physical Review Research* **6**, 043055 (2024).

[47] P. Padmanabha, G. Nicoletti, D. Bernardi, S. Suweis, S. Azaele, A. Rinaldo, and A. Maritan, Landscape and environmental heterogeneity support coexistence in competitive metacommunities, *Proc. Natl. Acad. Sci.* **121**, <https://doi.org/10.1073/pnas.2410932121> (2024).

[48] A. Doimo, G. Nicoletti, D. Bernardi, and P. Padmanabha, Finite-size scaling of survival statistics in metapopulation models, *Phys. Rev. E* **111**, 064415 (2025).

[49] C. W. Gardiner *et al.*, *Handbook of stochastic methods*, Vol. 3 (springer Berlin, 1985).

[50] A. J. McKane and T. J. Newman, Stochastic models in population biology and their deterministic analogs, *Phys. Rev. E* **70**, 041902 (2004).

[51] A. Lajmanovich and J. A. Yorke, A deterministic model for gonorrhea in a nonhomogeneous population, *Mathematical Biosciences* **28**, 221 (1976).

[52] A. Fall, A. Iggidr, G. Sallet, and J. J. Tewa, Epidemiological models and lyapunov functions, *Mathematical Modelling of Natural Phenomena* **2**, 62 (2007).

[53] R. Durrett and S. Levin, Spatial aspects of interspecific competition, *Theoretical Population Biology* **53**, 30 (1998).

[54] V. Calcagno, N. Mouquet, P. Jarne, and P. David, Coexistence in a metacommunity: the competition–colonization trade-off is not dead, *Ecology letters* **9**, 897 (2006).

[55] G. Meszéna, M. Gyllenberg, L. Pásztor, and J. A. Metz, Competitive exclusion and limiting similarity: A unified theory, *Theoretical Population Biology* **69**, 68 (2006).

[56] C. Violette, Z. Pu, and L. Jiang, Experimental demonstration of the importance of competition under disturbance, *Proceedings of the National Academy of Sciences* **107**, 12925 (2010).

[57] A. Posfai, T. Taillefumier, and N. S. Wingreen, Metabolic trade-offs promote diversity in a model ecosystem, *Physical review letters* **118**, 028103 (2017).

[58] M. Tikhonov and R. Monasson, Collective phase in resource competition in a highly diverse ecosystem, *Physical review letters* **118**, 048103 (2017).

[59] L. S. Comita, S. A. Queenborough, S. J. Murphy, J. L. Eck, K. Xu, M. Krishnadas, N. Beckman, and Y. Zhu, Testing predictions of the janzen–connell hypothesis: a meta-analysis of experimental evidence for distance- and density-dependent seed and seedling survival, *Journal of Ecology* **102**, 845 (2014).

[60] A. Sirén, P. Hambäck, and J. Machoa, Including spatial heterogeneity and animal dispersal when evaluating hunting: a model analysis and an empirical assessment in an amazonian community, *Conserv Biol* **18**, 1315 (2004).

[61] A. Ramette and J. M. Tiedje, Multiscale responses of microbial life to spatial distance and environmental heterogeneity in a patchy ecosystem, *Proceedings of the National Academy of Sciences* **104**, 2761 (2007).

[62] B. Zhang, D. L. DeAngelis, W.-M. Ni, Y. Wang, L. Zhai, A. Kula, S. Xu, and J. D. Van Dyken, Effect of stressors on the carrying capacity of spatially distributed metapopulations, *The American Naturalist* **196**, E46 (2020), pMID: 32673100.

- [63] A. Gandhi, S. Levin, and S. Orszag, “Critical Slowing Down” in time-to-extinction: an example of critical phenomena in ecology, *Journal of Theoretical Biology* **192**, 363 (1998).
- [64] G. Yaari, Y. Ben-Zion, N. M. Shnerb, and D. A. Vasseur, Consistent scaling of persistence time in metapopulations, *Ecology* **93**, 1214 (2012).
- [65] O. Ovaskainen and B. Meerson, Stochastic models of population extinction, *Trends in Ecology & Evolution* **25**, 643 (2010).
- [66] D. Bernardi and B. Lindner, Receiver operating characteristic curves for a simple stochastic process that carries a static signal, *Phys. Rev. E* **101**, 062132 (2020).
- [67] P. Padmanabha, S. Azaele, and A. Maritan, Generalisation of fluctuation-dissipation theorem to systems with absorbing states, *New J. Phys.* **25**, 113001 (2023).
- [68] D. A. Kessler and N. M. Shnerb, Extinction time distributions of populations and genotypes, *Phys. Rev. E* **108**, 044406 (2023).
- [69] J. Aguilar, M. A. Muñoz, and S. Azaele, The limits of inference in complex systems: When stochastic models become indistinguishable, arXiv <https://doi.org/10.48550/arXiv.2509.24977> (2025).
- [70] R. Tamme, I. Hiiresalu, L. Laanisto, R. Szava-Kovats, and M. Pärtel, Environmental heterogeneity, species diversity and co-existence at different spatial scales, *J Veg Sci* **21**, 796 (2010).
- [71] O. Allouche, M. Kalyuzhny, G. Moreno-Rueda, M. Pizarro, and R. Kadmon, Area–heterogeneity tradeoff and the diversity of ecological communities, *Proceedings of the National Academy of Sciences* **109**, 17495 (2012).
- [72] J. Hortal, L. M. Carrascal, K. A. Triantis, E. Thébaud, S. Meiri, and S. Sfenthourakis, Species richness can decrease with altitude but not with habitat diversity, *Proceedings of the National Academy of Sciences* **110**, <https://doi.org/10.1073/pnas.1301663110> (2013).
- [73] J. Carnicer, L. Brotons, S. Herrando, and D. Sol, Improved empirical tests of area-heterogeneity tradeoffs, *Proceedings of the National Academy of Sciences* **110**, <https://doi.org/10.1073/pnas.1222681110> (2013).
- [74] M. Hamm and B. Drossel, Habitat heterogeneity hypothesis and edge effects in model metacommunities, *Journal of Theoretical Biology* **426**, 40 (2017).
- [75] M. M. Herberich, S. Gayler, and K. Tielbörger, Environmental heterogeneity promotes coexistence among plant life-history strategies through stabilizing mechanisms in space and time, *Basic and Applied Ecology* **71**, 45 (2023).
- [76] Z. R. Miller and S. Allesina, Habitat heterogeneity, environmental feedbacks, and species coexistence across timescales, *The American Naturalist* **202**, E53 (2023), pMID: 37531282.
- [77] C. Xue and N. Goldenfeld, Coevolution maintains diversity in the stochastic “kill the winner” model, *Phys. Rev. Lett.* **119**, 268101 (2017).
- [78] J. Kang, S. Zhang, Y. Niu, F. Zhong, and X. Wang, Intraspecific predator interference promotes biodiversity in ecosystems, *eLife* **13**, <https://doi.org/10.7554/eLife.93115.3> (2024).
- [79] M. T. Pearce, A. Agarwala, and D. S. Fisher, Stabilization of extensive fine-scale diversity by ecologically driven spatiotemporal chaos, *Proceedings of the National Academy of Sciences* **117**, 14572 (2020).
- [80] A. Altieri and G. Biroli, Effects of intraspecific cooperative interactions in large ecosystems, *SciPost Physics* **12**, 013 (2022).
- [81] E. Mallmin, A. Traulsen, and S. De Monte, Chaotic turnover of rare and abundant species in a strongly interacting model community, *Proceedings of the National Academy of Sciences* **121**, e2312822121 (2024).
- [82] D. Bernardi, G. Nicoletti, P. Padmanabha, S. Suweis, S. Azaele, A. Rinaldo, and A. Maritan, A novel metric for species vulnerability and coexistence in spatially-extended ecosystems, arXiv <https://doi.org/10.48550/arXiv.2503.10288> (2025).

Appendix A: Proofs of theorems of Section III

Proof of Theorem 1. We begin by linearizing Eq. (15) around the extinction solution $\vec{p} = 0$, which yields

$$\dot{p}_i = -e_i p_i + \sum_{j=1}^N K_{ij} c_j p_j. \quad (\text{A1})$$

According to the Perron-Frobenius theorem, the eigenvalue of the generalized landscape matrix $\hat{\mathcal{M}} = \hat{K} \hat{\mathcal{C}} \hat{\mathcal{E}}^{-1}$ with the greatest modulus is real and positive, denoted by λ_{\max} , and we can associate with it a left eigenvector \vec{w} with strictly positive entries. We now consider the temporal evolution of $\vec{w}^T \vec{p}(t) \equiv f(t)$, the projection of \vec{p} onto \vec{w} . In the remainder of this proof, we drop the arrow symbols from vectors to reduce notation clutter. Since w is a left eigenvector of $\hat{\mathcal{M}}$ corresponding to the eigenvalue λ , we can write

$$w^T \hat{\mathcal{M}} = \lambda_{\max} w^T \quad \text{or, equivalently,} \quad w^T \hat{K} \hat{\mathcal{C}} = \lambda_{\max} w^T \hat{\mathcal{E}}. \quad (\text{A2})$$

We can make use of this last relation to obtain the following equation for the time derivative of $f(t)$

$$\dot{f} = -w^T \hat{\mathcal{E}} p + w^T \hat{K} \hat{\mathcal{C}} p = w^T \hat{\mathcal{E}} p (-1 + \lambda_{\max}), \quad (\text{A3})$$

We now define $e_{\min} > 0$ as the minimum local extinction rate, i.e. $e_{\min} \equiv \min\{e_i : i = 1, \dots, N\}$, and derive the following inequality:

$$w^T \hat{\mathcal{E}} p = \sum_i w_i p_i e_i \geq e_{\min} \sum_i w_i p_i = e_{\min} f. \quad (\text{A4})$$

If $\lambda_{\max} > 1$, multiplying the last inequality by $\lambda_{\max} - 1$ and combining with Eq. (A3) leads to:

$$\dot{f}(t) > e_{\min} (\lambda_{\max} - 1) f(t), \quad (\text{A5})$$

which implies

$$f(t) \geq f(0) e^{e_{\min} (\lambda_{\max} - 1) t}. \quad (\text{A6})$$

Thus $f(t)$ grows exponentially, which means at least one component $p_i(t)$ must increase, showing that the extinction state, $\vec{p} = 0$, is unstable. Consider now the case $\lambda_{\max} < 1$. From Eq. (15) one derives the following exact inequality ,

$$\dot{p}_i(t) \leq -e_i p_i + \sum_{j=1}^N K_{ij} c_j p_j. \quad (\text{A7})$$

Using the same steps as above we get

$$\dot{f} \leq w^T \hat{\mathcal{E}} p (\lambda_{\max} - 1) \leq e_{\min} (\lambda_{\max} - 1) f, \quad (\text{A8})$$

which implies

$$f(t) \leq f(0) e^{e_{\min} (\lambda_{\max} - 1) t}. \quad (\text{A9})$$

The exponential decay of $f(t) = \sum_i w_i p_i(t)$ – a sum of non negative terms – implies that $p_i(t) \rightarrow 0$ for all i as $t \rightarrow \infty$ since $w_i > 0 \ \forall i$. Hence, the extinction state, $\vec{p} = 0$, is globally stable. \square

Proof of Corollary 1. Let $\vec{p}^* \neq 0$ indicate a non-trivial stable stationary state of Eq. (15). Suppose $p_k^* = 0$ for an index k . Then, Eq. (15) implies that

$$\sum_{j=1}^N K_{kj} c_j p_j^* = 0. \quad (\text{A10})$$

This implies that $p_j^* = 0$ for all j such that $K_{kj} c_j > 0$. Because \hat{K} is irreducible, a positive integer $m(i)$ exists such that $(\hat{K}^m)_{ki} > 0$ for each i . Consequently, for each i there is at least one sequence of n elements of \hat{K} such that $K_{kk_{n-1}} K_{k_{n-1}k_{n-2}} \dots K_{k_1i} > 0$, $1 \leq n \leq m$, with $k, k_{n-1}, \dots, k_1, i$ being all distinct. Therefore, $p_{k_{n-1}}^* = 0$. We can now state Eq. (A10) with $p_{k_{n-1}}^*$ in place of p_k^* , which implies $p_{k_{n-2}}^* = 0$. We can do this recursively, obtaining $p_i^* = 0$. Since i is arbitrary we find that $\vec{p}^* = 0$, which contradicts the hypothesis that \vec{p}^* is non-trivial. \square

Proof of Corollary 2. We begin by noting that, if $c_i = cA_i$, $e_i = e/A_i$, and $K_{ij} = e^{-\alpha d_{ij}}$ the generalized landscape matrix can be written as

$$\mathcal{M}_{ij} = \frac{c}{e} \mathcal{M}_{ij}^H, \quad \mathcal{M}_{ij}^H \equiv A_i e^{-\alpha d_{ij}} A_j \quad (\text{A11})$$

where \mathcal{M}_{ij}^H is symmetric and is equivalent to the landscape matrix introduced by Hanski and Ovaskainen [4]. Thus, since $\delta = e/c$, the “leading eigenvalue” or “metapopulation capacity” of $\hat{\mathcal{M}}^H$ is $\lambda_M = \delta \cdot \lambda_{\max}$. Hence, the condition $\lambda_{\max} > 1$ is equivalent to $\lambda_M > \delta$. \square

Proof of Theorem 2. The matrix $\hat{K}\hat{\mathcal{E}}^{-1}$ is irreducible. Let \tilde{K}_0 be the row sum of \hat{K} , which is row-independent. Then, $\vec{v} = (1, \dots, 1)^T$ is a right eigenvector of \hat{K} corresponding to the eigenvalue \tilde{K}_0 . For non-negative matrices, the spectral radius is bounded by the minimum and maximum row sums from above and below, respectively. Hence, we conclude that \vec{v} is the Perron-Frobenius eigenvector of both \hat{K} and $\hat{K}\hat{\mathcal{E}}^{-1}$, since $\hat{\mathcal{E}}$ is a scalar matrix. Hence, from Theorem 1 we conclude that: if $\tilde{K}_0/e < 1$ the absorbing state $p_x^* = 0$ is globally stable; if $\tilde{K}_0/e > 1$ the absorbing state is unstable, and $p_x^* = 1 - e/\tilde{K}_0$ is a stationary state.

To show that $p_x^* = 1 - e/\tilde{K}_0$ is the only stationary state, assume that $s_x > 0$ is a non-trivial steady state of the dynamics Eq. (18). Then, we can write

$$\frac{1}{s_x} = 1 + \frac{e}{\sum K_{xy} s_y}. \quad (\text{A12})$$

Define now $P = \min s_x$ and $Q = \max s_x$. Clearly, $0 < P \leq Q$, and

$$1 + \frac{e}{\tilde{K}_0 Q} \leq \frac{1}{s_x} \leq 1 + \frac{e}{\tilde{K}_0 P}. \quad (\text{A13})$$

Since the first inequality must hold for all x , we can evaluate it for the index for which $s_{x_Q} = Q$, obtaining

$$1 + \frac{e}{\tilde{K}_0 Q} \leq \frac{1}{s_{x_Q}} = \frac{1}{Q}. \quad (\text{A14})$$

Doing the same for the second inequality in Eq. (A13) and combining with $1/Q \leq 1/P$ yields

$$1 + \frac{e}{\tilde{K}_0 Q} \leq \frac{1}{Q} \leq \frac{1}{P} \leq 1 + \frac{e}{\tilde{K}_0 P}. \quad (\text{A15})$$

The first and last inequalities imply

$$Q \leq 1 - \frac{e}{\tilde{K}_0} \quad \text{and} \quad 1 - \frac{e}{\tilde{K}_0} \leq P, \quad (\text{A16})$$

respectively. The two last equalities are only consistent with $P \leq Q$ if $P = Q = s_x = 1 - \frac{e}{\tilde{K}_0}$. This shows that $p_x^* = 1 - e/\tilde{K}_0$ is the only stationary solution. We now prove its linear stability by studying explicitly the eigenvalues of the Jacobian matrix evaluated at $p_x^* = p^* = 1 - e/\tilde{K}_0$

$$J_{xy} = \frac{\partial \dot{p}_x}{\partial p_y} \bigg|_{p^*} = (-e + \tilde{K}_0 p^*) \delta_{xy} + (1 - p^*) K_{xy} \quad (\text{A17})$$

$$= \tilde{K}_0 \delta_{xy} + \frac{e}{\tilde{K}_0} K_{xy}. \quad (\text{A18})$$

If λ_α indicate the eigenvalues of \hat{K} , the eigenvalues of the Jacobian matrix are $\frac{e}{\tilde{K}_0} \lambda_\alpha - \tilde{K}_0$. We have shown above that $\max_\alpha \operatorname{Re}\{\lambda_\alpha\} = \tilde{K}_0$. Hence, the eigenvalue with the maximum real part is $e - \tilde{K}_0 < 0$, which implies the linear stability of the equilibrium. \square

Alternative proof of Theorem 2 based on Fourier modes. We consider the uniform stationary state $p_i = p^*$ for all i , in which all patches have the same population. We consider the global extinction solution $p^* = 0$ first, which is always a fixed point of the system Eq. (18). We then considered the system's linearization around it:

$$\dot{p}_i = -ep_i + \sum_{j \in \Lambda} K_{ij} p_j. \quad (\text{A19})$$

Because we dealing with a linear, translation invariant system, plain waves $\mathbf{v}_k = (e^{i2\pi k \cdot j/N})_{j=0,1,\dots,N-1}$ with $k \in \{0, \dots, N-1\}^d$ represent a full set of eigenfunctions, or modes. Thus $\mathbf{p}(t) = \sum_{k=0}^{N-1} a_k(t) \mathbf{v}_k$ where the mode's amplitude response can be computed using Eq. (A19), leading to

$$\dot{a}_k = (-e + \tilde{K}_k) a_k, \quad (\text{A20})$$

where $\tilde{K}_k = \sum_j e^{-i2\pi k j / N} K_{ij}$ indicates the discrete Fourier transform of the kernel \hat{K} . Equation (A20) is solved by an exponential function, which decays to zero when $-e + \operatorname{Re}\{\tilde{K}_k\} < 0$. Requiring $\max_k \operatorname{Re}\{\tilde{K}_k\} < e$ guarantees then that the amplitude of all modes decays, and that the extinction equilibrium is thus stable. Since $\operatorname{Re}\{\tilde{K}_k\} = \sum_j K_{ij} \cos(2\pi k j / N) \leq \sum_j K_{ij} = \tilde{K}_0$, then $\max_k \operatorname{Re}\{\tilde{K}_k\} = \tilde{K}_0$, we conclude that $\tilde{K}_0 < e$ implies the local stability of $p^* = 0$, which proves the first part of the theorem. Naturally, this condition is consistent with Theorem 1, because $\tilde{K}_0 = \lambda_M$ is the largest eigenvalue of the dispersal kernel.

To prove the second part of the theorem, we begin with determining the nonzero uniform fixed point from Eq. (A19):

$$p^* = \frac{\tilde{K}_0 - e}{\tilde{K}_0}. \quad (\text{A21})$$

First, we notice that Eq. (A21) is unfeasible when $e > \tilde{K}_0$, i.e., when the trivial solution is stable. Conversely, the nontrivial solution is feasible when $e < \tilde{K}_0$. To study its stability, we compute the Jacobian matrix and evaluate it at $p_i = p^*$:

$$J_{\ell j} = \frac{d\dot{p}_\ell}{dp_j} \bigg|_{p^*} = \delta_{\ell j} \left(-e - \tilde{K}_0 p^* \right) + (1 - p^*) K_{\ell j}, \quad (\text{A22})$$

which has the following eigenvalues

$$(-e - \tilde{K}_0 p^*) + (1 - p^*) \tilde{K}_k. \quad (\text{A23})$$

For the fixed point to be stable, all eigenvalues must have a negative real part. In other words, the largest real part must be negative, i.e.

$$0 > \max_k \left\{ (-e - \tilde{K}_0 p^*) + (1 - p^*) \tilde{K}_k \right\} = -e - \tilde{K}_0 p^* + (1 - p^*) \tilde{K}_0 = e - \tilde{K}_0, \quad (\text{A24})$$

which proves the second part of the theorem. \square

Appendix B: Proofs of theorems of Section VI

Proof of Theorem 3. We begin with noting that if \hat{K}_α is translation-invariant, then so is $c_\alpha \hat{K}_\alpha$. Hence, we can consider the case $c_\alpha = 1$, which amounts to a redefinition of $K_{\alpha,ij}$ that does not change the theorem's hypotheses. We now consider the uniform stationary solution, i.e. $p_{\alpha,i}^* = p_\alpha^*$ for all i , and introduce $Q \equiv 1 - \sum_{\beta=1}^S p_\beta^*$, so that a uniform stationary solution to Eq. (36) must satisfy

$$e_\alpha p_\alpha^* = Q \sum_{j=1}^N K_{\alpha,ij} p_\alpha^*. \quad (\text{B1})$$

If species α survives, then $p_\alpha^* > 0$, which implies

$$\frac{e_\alpha}{z_\alpha} = Q, \quad (\text{B2})$$

where we introduced the shorthand for the zero-frequency Fourier mode of \hat{K}_α

$$z_\alpha \equiv \sum_j K_{\alpha,ij} = \tilde{K}_{\alpha,0}, \quad (\text{B3})$$

and $Q \in (0, 1)$. Equation (B2) must hold for any species that survives. Hence, given the set E , one of the 2^S possible subsets of the S species, a spatially uniform solution in which all species within E coexist is defined by:

$$\mathcal{C} = \{\mathbf{p}^* : p_{\alpha i} \equiv p_\alpha^* \text{ if } \alpha \in E, p_{\alpha i} = 0 \text{ if } \alpha \notin E \text{ and } \sum_\alpha p_\alpha^* + Q - 1 = 0\} \quad (\text{B4})$$

We now show that \mathcal{C} is a center manifold. To this end, we first compute the system's Jacobian, \hat{J} , from Eq. (36), and evaluate it at a point belonging to \mathcal{C} :

$$\left. \frac{d\hat{p}_{\alpha i}}{dp_{\beta k}} \right|_{\mathbf{p}^* \in \mathcal{C}} = J_{(\alpha,i),(\beta,k)} = -\delta_{ik} \delta_{\alpha\beta} e_\alpha + \left(1 - \sum_\nu p_\nu^* \right) K_{\alpha,ik} \delta_{\alpha\beta} - \delta_{ik} \sum_\ell K_{\alpha,i\ell} p_\alpha^* \quad (\text{B5})$$

$$= -\delta_{ik} \delta_{\alpha\beta} e_\alpha + Q K_{\alpha,ik} \delta_{\alpha\beta} - \delta_{ik} p_\alpha^* z_\alpha. \quad (\text{B6})$$

To prove that \mathcal{C} is a center manifold, we consider the following set:

$$\mathcal{C}_0 = \{\mathbf{v} : v_{\alpha i} \text{ independent of } i \text{ and } \sum_\alpha v_{\alpha i} = 0\}. \quad (\text{B7})$$

According to this definition, a vector $\mathbf{v} \in \mathcal{C}_0$ is uniform with respect to the patch index, and the sum over species index is null, i.e., $\sum_\alpha v_{\alpha i} = 0$. Applying the Jacobian to $\mathbf{v} \in \mathcal{C}_0$ demonstrates directly that \mathbf{v} is an eigenvector of \hat{J} corresponding to the zero eigenvalue (we write $v_{\beta k} = v_\beta$ for simplicity, since the components of \mathbf{v} cannot depend on the patch index):

$$\begin{aligned} \sum_{\beta,k} J_{(\alpha,i),(\beta,k)} v_{\beta,k} &= -\sum_\beta \sum_k \delta_{\alpha\beta} \delta_{ik} e_\alpha v_\beta + Q \sum_\beta \sum_k K_{\alpha,ik} \delta_{\alpha\beta} v_\beta + \sum_{\beta,k} p_\alpha^* z_\alpha v_\beta \\ &= v_\alpha (-e_\alpha + z_\alpha Q) - p_\alpha^* z_\alpha \sum_\beta v_\beta = 0. \end{aligned}$$

We conclude that the Jacobian has a nontrivial null space, which implies that \mathcal{C} is a center manifold.

We now prove the stability of \mathcal{C} . To this end, we first show that there are no positive eigenvalues. To begin with, we note that the Jacobian has a block structure, in which each of the S diagonal blocks, indexed by α , is $Q\hat{K}_\alpha - e_\alpha I_N + \hat{p}_\alpha$, where $\hat{p}_\alpha = -p_\alpha^* z_\alpha$. Each off-diagonal block is $I_N \hat{p}_\alpha$, where α is the row index, and off-diagonal blocks do not depend on the block column index. We define $U \in \mathbb{C}^{N \times N}$ as the basis change matrix that diagonalizes every block (a spatial plain wave basis), i.e. each column of U is $e^{iq\ell}$ and q is the wave number. We can write for the entire block matrix

$$P = \text{diag}(U, \dots, U) = I_S \otimes U \quad (P^{-1} = P^\dagger). \quad (\text{B8})$$

We apply this similarity transformation to the Jacobian matrix,

$$\tilde{J} := P^{-1}JP = [\tilde{J}(q)]_{q=0}^{N-1}, \quad (\text{B9})$$

which splits the problem into the Fourier modes $\tilde{J}(q) \in \mathbb{C}^{S \times S}$ (the basis change has no effect on the off-diagonal blocks because they are scalar matrices). Explicitly, we find a Jacobian for each mode, which is

$$\tilde{J}_{\alpha\beta}(q) = (Q\lambda_{K_\alpha}(q) - e_\alpha + \hat{p}_\alpha) \delta_{\alpha\beta} + \hat{p}_\alpha (1 - \delta_{\alpha\beta}) \quad (\text{B10})$$

with block (species) indices $\alpha, \beta = 1, \dots, S$ and $\lambda_{K_\alpha}(q)$ is the q eigenvalue from each \hat{K}_α . We now set

$$d_\alpha(q) := Q\lambda_{K_\alpha}(q) - e_\alpha, \quad u_\alpha := \hat{p}_\alpha, \quad \mathbf{1} := (1, \dots, 1)^\top, \quad (\text{B11})$$

so that we split the matrix into two parts:

$$\tilde{J}(q) = D(q) + u \mathbf{1}^\top, \quad (\text{B12})$$

where $D_{\alpha\beta}(q) = d_\alpha(q) \delta_{\alpha\beta}$ is diagonal and the other term has a rank one. We now look for the eigenvalues of $\tilde{J}(q)$, which are the zeros of the equation

$$\det(\tilde{J}(q) - \mu I_S) = \det(D(q) - \mu I_S) \left[1 + \mathbf{1}^\top (D(q) - \mu I_S)^{-1} u \right], \quad (\text{B13})$$

where we used the matrix determinant lemma. Since $D(q)$ is diagonal, the term in square brackets is easy to compute, which yields

$$\mathbf{1}^\top (D(q) - \mu I_S)^{-1} u = \sum_{\alpha=1}^S \frac{\hat{p}_\alpha}{d_\alpha(q) - \mu}. \quad (\text{B14})$$

Hence, the characteristic equation to find the eigenvalues becomes

$$\det(\tilde{J}(q) - \mu I_S) = \prod_{\alpha=1}^S [d_\alpha(q) - \mu] f_q(\mu) = 0 \quad (\text{B15})$$

where

$$f_q(\mu) := 1 + \sum_{\alpha=1}^S \frac{\hat{p}_\alpha}{d_\alpha(q) - \mu}. \quad (\text{B16})$$

Recalling that $\lambda_{K_\alpha}(0) = z_\alpha$, we now find for $q = 0$ that

$$d_\alpha(0) = Q\lambda_{K_\alpha}(0) - e_\alpha = e_\alpha \left(\frac{\lambda_{K_\alpha}(0)}{z_\alpha} - 1 \right) = 0. \quad (\text{B17})$$

Hence, the characteristic equation has a zero root with multiplicity $S - 1$, and the only non-zero root of the characteristic equation is

$$f_0(\mu) = 1 + \sum_{\alpha=1}^S \frac{\hat{p}_\alpha}{-\mu} = 0 \rightarrow \bar{\mu}_0 = \sum_{\alpha} \hat{p}_\alpha = - \sum_{\alpha} z_\alpha p_\alpha^* < 0. \quad (\text{B18})$$

Hence, the dominant eigenvalue for $q = 0$ is zero. Recalling the definition of $d_\alpha(q)$, Eq. (B11), we now consider $q \neq 0$, and observe that

$$d_\alpha(q) < d_\alpha(0) = 0 \quad (\text{B19})$$

where the inequality holds because \hat{K}_α is positive and translation invariant, a fact used also in Theorem 2. Assuming now that species are different, then $d_\alpha(q)$ are distinct when $q \neq 0$. Direct substitution shows that none of $d_\alpha(q)$ are zeros of the characteristic equation. Hence, all non-uniform eigenvalues are roots of $f_q(\mu)$. We now take the real part of $f_q(\mu)$

$$\text{Re}\{f_q(\mu)\} = 1 + \sum_{\alpha=1}^S \hat{p}_\alpha \frac{\text{Re}\{d_\alpha(q)\} - \text{Re}\{\mu\}}{|d_\alpha(q) - \mu|^2}, \quad (\text{B20})$$

and assume that $\text{Re}\{\mu\} \geq 0$. Then, using Eq. (B19) and recalling that $\hat{p}_\alpha < 0$ for all α , we conclude that all terms in the sum are positive. Hence, the real part of $f_q(\mu)$ is always strictly larger than one, and cannot have any root in the $\text{Re}\{f_q(\mu)\} \geq 0$ half plane when $q \neq 0$. We conclude that all eigenvalues for $q \neq 0$ have strictly negative real part. Hence, the maximum eigenvalue is zero and has with multiplicity $S - 1$, which defines the center manifold introduced above.

Finally, we compute the system's response to a small perturbation from one point belonging to the center manifold \mathcal{C} , keeping all nonlinear terms. We insert

$$p_{\alpha i} = p_\alpha^* + \Delta p_{\alpha i} \quad (\text{B21})$$

into the equations of motion, obtaining

$$\dot{p}_{\alpha i} = \Delta \dot{p}_{\alpha i} = -e_\alpha (p_\alpha^* + \Delta p_{\alpha i}) + \left[1 - \sum_{\beta} (p_\beta^* + \Delta p_{\beta i}) \right] \sum_j K_{\alpha,ij} (p_\alpha^* + \Delta p_{\alpha j}) \quad (\text{B22})$$

$$= -e_\alpha p_\alpha^* - e_\alpha \Delta p_{\alpha i} + \underbrace{\left(1 - \sum_{\beta} p_\beta^* \right)}_{Q} \sum_j K_{\alpha,ij} (p_\alpha^* + \Delta p_{\alpha j}) \quad (\text{B23})$$

$$- \sum_{\beta} \Delta p_{\beta i} \sum_j K_{\alpha,ij} (p_\alpha^* + \Delta p_{\alpha j}) \quad (\text{B24})$$

$$= -e_\alpha p_\alpha^* - e_\alpha \Delta p_{\alpha i} + Q \underbrace{\sum_j K_{\alpha,ij} p_\alpha^*}_{z_\alpha} + Q \sum_j K_{\alpha,ij} \Delta p_{\alpha j} \quad (\text{B25})$$

$$- \sum_{\beta} \Delta p_{\beta i} \sum_j K_{\alpha,ij} p_\alpha^* + \sum_{\beta} \Delta p_{\beta i} \sum_j K_{\alpha,ij} \Delta p_{\alpha j} \quad (\text{B26})$$

$$= \sum_{\beta,j} J_{(\alpha,i),(\beta,j)} \Delta p_{\beta j} - \sum_j K_{\alpha,ij} \Delta p_{\alpha j} \sum_{\beta} \Delta p_{\beta i}. \quad (\text{B27})$$

Consistently, the constant term vanishes, the linear term coincides with the Jacobian, and the only nonlinear part is quadratic.

It is easy to see that the eigenvectors corresponding to the zero eigenvalue span the $S - 1$ dimensional space defined by the \mathcal{C}_0 set defined above. For any $v \in \mathcal{C}_0$, the linear and quadratic responses are zero,

and since there are no higher order terms, we conclude that any perturbation along this direction does not feel any response field, and does not leave \mathcal{C} . For perturbations along any other direction, the linear term dominates, and acts hence as a restoring force. \square

Proof of Theorem 4. When $p_\alpha^* = p_1^* \delta_{\alpha 1}$, the Jacobian Eq. (B5) is upper block triangular, so its eigenvalues are those of the diagonal blocks. The block corresponding to the surviving species $\alpha = 1$ is $(-e_1 - z_1 p_1^*) \mathbb{I}_N + Q \hat{K}_1$, with $Q = e_1/z_1$, $p_1^* = 1 - e_1/z_1$, and $\hat{K}_1 = (K_{1,ij})$. Since \hat{K}_β is positive for all β (irreducible would suffice), its largest eigenvalue $\lambda_{M,1}$ is bounded between the minimum and maximum row sums. Translational invariance makes the row sum constant, z_1 , so $\lambda_{M,1} = z_1$. The largest eigenvalue of this block is $(-e_1 - z_1(1 - e_1/z_1)) + (e_1/z_1) \cdot z_1 = e_1 - z_1 < 0$. For each extinct species $\alpha \neq 1$, Eq. (B5) with $\alpha = \beta$ gives the block $-e_\alpha \mathbb{I}_N + Q \hat{K}_\alpha$, where again $Q = e_1/z_1$. Its largest eigenvalue is $-e_\alpha + (e_1/z_1) z_\alpha < -e_\alpha + (e_\alpha/z_\alpha) z_\alpha = 0$, where the inequality follows from the hypothesis $e_1/z_1 < e_\alpha/z_\alpha$ for all $\alpha \neq 1$. Since all blocks have strictly negative leading eigenvalues, the state $p_\alpha^* = p_1^* \delta_{\alpha 1}$ is locally stable. \square

Appendix C: Derivation of stochastic dynamics

We refer to Ref. [48] for a detailed derivation of the reduced SDE. Briefly, we start from the two-dimensional Fokker–Planck equation (19) for the joint probability density $\mathcal{P}(\vec{p}, \vec{x}, t)$, we derive the one-dimensional stochastic dynamics for the effective settled population density ρ . To reduce dimensionality, we begin by assuming a fully connected dispersal network and homogeneous habitat patches ($c_i = c$, $e_i = e \forall i$), rendering the system translationally invariant. Setting $\mathcal{A} = 1/N$ ensures a well-defined large- N limit. By integrating out all sites except one, we define the marginalized probability distribution $P(\rho, x, t)$. Under mean-field–like approximations consistent with the fully connected topology, each variable is replaced by its effective value. In the limit $N \rightarrow \infty$, this procedure yields a two-dimensional Fokker–Planck equation for $P(\rho, x, t)$, governing the joint stochastic dynamics of the settled and explorer effective population densities ρ, x .

By subsequently invoking a separation of timescales between the dynamics of explorers and settled populations, which we apply to the corresponding Langevin formulation, we obtain the following one-dimensional effective Itô SDE:

$$\dot{\rho} = \tilde{\mathcal{A}}(\rho) + \sqrt{\frac{1}{M} \tilde{\mathcal{D}}(\rho)} \sigma(t), \quad \tilde{\mathcal{A}}(\rho) = [c h(f) (1 - \rho) - e] \rho, \quad \tilde{\mathcal{D}}(\rho) = e + \frac{ch(f)}{2(1+D/\lambda)} [1 - \rho^2 + 2\frac{D}{\lambda} (1 - \rho)] \quad (C1)$$

The drift $\tilde{\mathcal{A}}(\rho)$ coincides with the deterministic mean-field dynamics (4), while the diffusion term $\tilde{\mathcal{D}}(\rho)$ arises from the combination of demographic noise in both the explorer and settled compartments, properly renormalized by the fast-variable elimination.

To derive the scaling relations presented in Section IV, we start from the backward Fokker–Planck equation corresponding to Eq. (23) for the n -th moment of extinction time $T_n = \langle T^n \rangle$ reads:

$$\tilde{\mathcal{A}}(\rho) \partial_\rho T_n(\rho) + \frac{1}{2M} \tilde{\mathcal{D}}(\rho) \partial_\rho^2 T_n(\rho) = -n T_{n-1}(\rho) \quad (C2)$$

and that for the survival probability:

$$\partial_t S = \tilde{\mathcal{A}}(\rho) \partial_\rho S + \frac{1}{2M} \tilde{\mathcal{D}}(\rho) \partial_\rho^2 S. \quad (C3)$$

Introducing the parameter

$$\Delta = \frac{1}{\lambda_M} \left(\lambda_M - \frac{e}{c} \right) = \frac{\epsilon}{\lambda_M}, \quad (C4)$$

to quantify the distance from the transition point, $\tilde{\mathcal{A}}$ and $\tilde{\mathcal{D}}$ can be rewritten as:

$$\begin{aligned} \tilde{\mathcal{A}}(\rho, M, \Delta) &= \lambda_M c (\Delta - \rho) \rho \\ \tilde{\mathcal{D}}(\rho, M, \Delta) &= \frac{\lambda_M c}{2} \left[3 + \frac{D}{D + \lambda} - 2\Delta - \frac{2D}{D + \lambda} \rho - \frac{\lambda}{D + \lambda} \rho^2 \right] \rho \end{aligned} \quad (C5)$$

α	ϕ	γ	η	β	δ
0	$-\frac{1}{2}$	$\frac{1}{2}$	$\frac{1}{2}$	$\frac{1}{2}$	1

TABLE I. Scaling exponents characterizing the survival probability S and the first and second moments of the exit time, $\langle T \rangle$ and $\langle T^2 \rangle$ in the vicinity of the critical point.

and we assume to be close to the transition point, so $\epsilon \approx 0$ in Eq. (C4).

By properly rescaling the effective population density $\rho \rightarrow \hat{\rho} = \rho \sqrt{M}$, the distance from the critical point $\Delta \rightarrow \hat{\Delta} = \Delta \sqrt{M}$ and the extinction-time moments in equation (C2) (or equivalently rescaling the survival probability in equation (C3)), we obtain the scaling exponents of I, which define the following scaling forms:

$$\begin{aligned} S(t|M) &= t^{-\alpha} \hat{S}(tM^\phi) \\ T_1(\rho, \Delta, M) &= M^\beta \hat{T}_1(\rho M^\gamma, \Delta M^\eta) . \\ T_2(\rho, \Delta, M) &= M^\delta \hat{T}_2(\rho M^\gamma, \Delta M^\eta) \end{aligned} \quad (\text{C6})$$

The scaling analysis above characterizes the critical behavior and extinction dynamics close to the transition point. Beyond this regime, in the survival phase ($\epsilon > 0$), the system reaches a metastable state where demographic fluctuations persist around a finite mean occupancy. To quantify these fluctuations and connect them with the underlying nonlinear stochastic dynamics, we next consider a linearized approximation around the deterministic fixed point. This approach leads to an Ornstein–Uhlenbeck (OU) description of the quasi-stationary dynamics,

$$\dot{\rho}_{\text{OU}} = -\kappa \rho_{\text{OU}} + \sqrt{2\sigma_{\text{eff}}} \eta(t), \quad \text{with} \quad \sigma_{\text{eff}} = \sqrt{\frac{D_{\text{eff}}}{2M\kappa}}, \quad (\text{C7})$$

where $\eta(t)$ is Gaussian white noise, and the effective drift κ and diffusion coefficient D_{eff} are

$$\kappa = \left| \frac{\partial \tilde{\mathcal{A}}}{\partial \rho} \Big|_{\rho_*} \right| = |e - c h(f)|, \quad D_{\text{eff}} = \tilde{\mathcal{D}}(\rho_*) = \frac{1}{2} \frac{e [e - c h(f)][e \lambda - 4 c h(f)(D + \lambda)]}{[c h(f)]^2 (D + \lambda)}. \quad (\text{C8})$$